# Hip fractures

## A biomechanical analysis of fracture strength prediction, prevention, and repair

Kok, Joeri

2021

*Document Version:*
Publisher's PDF, also known as Version of record

# Hip fractures

## A biomechanical analysis of fracture strength prediction, prevention, and repair

Joeri Kok

LUND UNIVERSITY

DOCTORAL DISSERTATION

by due permission of the Faculty of Engineering, Lund University, Sweden.
To be defended at the lecture hall *Belfragesalen, BMC, D15, Lund, Sweden*.
Friday, October 1st, 2021 at 9.00.

*Faculty opponent*
Prof. Harry van Lenthe
KU Leuven

Cover artwork by Joeri Kok depicting the proximal part of an intact and a fractured femur.

Department of Biomedical Engineering
Lund University
P.O. Box 118, SE-221 00 Lund
Sweden

ISBN: 978-91-8039-010-1 (print)

ISBN: 978-91-8039-011-8 (pdf)

ISRN-nr: LUTEDX/TEEM-1125-SE

Report No. 3/21


Printed in September 2021 by Tryckeriet i E-huset, Lund, Sweden

**Public defence**

October, 1st, 2021, 9.00 in Belfragesalen
BMC D15, Lund University, Sölvegatan 17, 222 42 Lund, Sweden

**Supervisors**

Prof. Hanna Isaksson
*Department of Biomedical Engineering*
*Lund University, Lund, Sweden*

Dr. Lorenzo Grassi
*Department of Biomedical Engineering*
*Lund University, Lund, Sweden*

**Faculty opponent**

Prof. Harry van Lenthe
*Department of Mechanical Engineering*
*Katholieke Universiteit Leuven, Leuven, Belgium*

**Board of examination**

Prof. Svein Kleiven
*Department of Biomedical Engineering and Health Sciences*
*Royal Institute of Technology (KTH), Stockholm, Sweden*

Prof. Cecilia Persson
*Department of Engineering Sciences, Applied Materials Science*
*Uppsala University, Uppsala, Sweden*

Prof. Björn Rosengren
*Department of Clinical Sciences Malmö, Orthopedics*
*Lund University, Lund, Sweden*

Deputy member: Assoc. Prof. Christina Bjerkén
*Department of Materials Science and Applied Mathematics*
*Malmö University, Malmö, Sweden*

Deputy member: Prof. Dmytro Orlov
*Department of Mechanical Engineering Sciences*
*Lund University, Lund, Sweden*

| | |
|---|---|
| **Organization**<br>LUND UNIVERSITY<br>Department of Biomedical Engineering<br>Box 118, 211 00 Lund, Sweden | **Document name**<br>DOCTORAL DISSERTATION<br>**Date of issue**<br>October 1, 2021 |
| Author: Joeri Kok | Sponsoring organization |


**Title and subtitle** Hip fractures - A biomechanical analysis of fracture strength prediction, prevention, and repair


**Abstract**

Due to the aging population, hip fracture incidence has been increasing over the past decades. Measurements of bone mineral density with dual energy X-ray absorptiometry are the gold standard for hip fracture risk assessment, where patients with a low bone density have a high risk of fracture. However, many people that are not diagnosed to be at risk, still fracture their hip. Calculations of bone strength using subject-specific finite element (FE) models, can improve fracture risk prediction, but further improvement is required.

Patients with a high fracture risk are often prescribed pharmaceutical treatment in order to increase bone density systemically. As systemic response to treatment is limited, other options to prevent fractures by improving the bone strength are investigated. One of those options is the injection of biomaterials in the femoral neck. In case of a hip fracture due to a low-energy fall, total hip replacement is generally preferred over joint-preserving methods like fixation using a dynamic hip screw. Screw fixation comes with a risk of screw instability, especially in low-density bone. Bone cements can be used to improve fixation of orthopaedic implants and fracture fixation devices. Calcium sulphate/hydroxyapatite (CaS/HA) is an injectable biomaterial that has been used, for example, to reinforce collapsed vertebrae and to stabilize wrist fractures.

The work presented in the thesis aims to improve fracture risk prediction, and fracture prevention and repair methods with use of CaS/HA. This is achieved through a combination of experimental mechanical tests at organ and tissue scale, and development and thorough validation of FE models of the proximal femur.

In the first part of this thesis, 12 cadaveric femora were used in an experiment where the bones were loaded until fracture in a configuration developed to replicate a fall to the side. During loading, high-speed cameras were used to image both the medial and lateral side of the femoral neck allowing for full-field strain measurements using digital image correlation. The femora were imaged with clinical CT before and micro-CT before and after mechanical testing. Using the acquired CT images, FE models were developed at two different resolutions to determine their ability to capture the fracture force, fracture location and surface strains. The FE models based on the clinical CT images were able to accurately capture the fracture force and identify regions where the bone would fracture. These models could also capture the strains with high accuracy. However, the strains were not predicted as accurately in regions with high surface irregularity. The models based on the micro-CT images could show with higher accuracy how the strains were distributed around local porosity (e.g., due to vascularization) in the femoral neck and how these influenced the fracture pattern.

The thesis continues with an investigation of fracture prevention and repair methods through the use of CaS/HA. The ability of CaS/HA to increase the fracture strength of the proximal femur for fracture prevention and its ability to stabilize a dynamic hip screw used for fracture repair was investigated. The increase in fracture strength was investigated using FE models. These models showed that CaS/HA can increase the fracture strength of the femur approximately 20% when injected close to the cortex in the lateral neck. Pullout tests using a dynamic hip screw were performed on synthetic bone blocks and femoral heads from hip fracture patients. In the synthetic blocks, CaS/HA significantly increased the pullout strength. However, in the human bone the stability of the screw was not improved, because the cement could not easily spread into the threads of the screws. The mechanical behaviour of CaS/HA and bone was further investigated using high-resolution synchrotron X-ray tomography. Cylindrical trabecular bone specimens with and without CaS/HA were imaged with tomography during in-situ loading of the samples. The images revealed that CaS/HA reinforced the bone, and that CaS/HA is a brittle material that will crack before the bone.

To conclude, in this thesis FE models are presented showing accurate prediction of fracture strength, which can be used for improved fracture risk assessments. Furthermore, the work provides insight in how CaS/HA behaves mechanically and how it can be used to increase the fracture strength and to stabilize fixation devices in the femur, improving fracture prevention and fracture repair methods.



**Key words:** Finite element, Bone cement, Femur, Fracture, Experimental Mechanics, X-ray Imaging

Classification system and/or index terms (if any)

| | |
|---|---|
| Supplementary bibliographical information<br>ISRN: LUTEDX/TEEM-1125-S<br>Report No. 3/21 | **Language:** English<br>**ISBN:** 978-91-8039-010-1 (print)<br>**ISBN:** 978-91-8039-011-8 (pdf) |

| | | |
|---|---|---|
| Recipient's notes | **Number of pages** | Price |
| | Security classification | |




Signature  Date 2021-08-29

# Popular science summary

The world's population is aging. In elderly, the bone density gradually decreases, and this process is accelerated in women after menopause. Low bone density increases the risk of hip fractures, which means that every year more and more people fracture their hip. To reduce the number of fractures, it is important that people at high risk are identified before the first fracture. Currently, risk is determined by measuring bone density using a 2D radiographic image. The work in this thesis is based on the hypothesis that a better way to assess risk would be to use 3D computer models that calculate the strength of the hip. One of the aims in this thesis is to develop computer models and accurately validate them against experimental mechanical tests that replicate a fall to the side.

When a patient is determined to be at high risk of fracture, they are prescribed pharmacological drugs to reduce further bone loss. These drugs are effective but have a limited ability to promote new bone formation. Orthopaedic surgeons use bone cements to, for example, stabilize implants or reinforce collapsed vertebrae. In the hip, it is thought that bone cements can be used to prevent fractures. Calcium sulphate/hydroxyapatite (CaS/HA) is a bone cement that is similar to bone itself. This cement has already been used for various orthopaedic purposes, which showed that the body is able to degrade and turn the cement into new bone. However, the mechanical properties need to be further characterised in detail. Patients that suffered a hip fracture due to low bone density often receive a total hip replacement. Another option is to fix the fracture with a dynamic hip screw, which is used to connect and stabilize the fractured pieces. These screws loosen easily in patients with low bone density but can be stabilized using bone cement. One of the aims in this thesis is to investigate how hip fractures can be prevented and better repaired with the use of CaS/HA.

The thesis starts with an investigation of the mechanical behaviour of the hip. Bones from human donors were loaded until they fractured in a way replicating a fall to the side. To get accurate measurements of the deformation of the bone, high-speed cameras were used to image the bone. Following the experiments, 3D computer models were created of these bones. Models were either created from clinical CT scans or from micro-CT scans with higher resolution. The

models built from clinical CT scans were able to accurately predict the force at which the bones would fracture and where they would fracture. The deformation was predicted with high accuracy, although the accuracy declined in regions where the surface of the bones was more irregular. With the micro-CT based models, it was possible to model the surface with greater accuracy and include irregularities on the surface. These models showed how the local deformations and resulting cracks are influenced by the irregularities on the surface of the bone.

The thesis continues with an investigation of fracture prevention and repair methods with use of CaS/HA. The ability of CaS/HA to strengthen the neck of the thighbone was shown using 3D computer models. The amount that the bone was strengthened highly depended on the region where bone cement was injected. Additionally, mechanical tests were performed to investigate if an injection of CaS/HA at the tip of a dynamic hip screw could increase stability of the screw. This was tested by inserting screws with and without CaS/HA into synthetic and human bone. By testing the force required to pull the screws out of the bones it was found that the CaS/HA helped stabilize the screw in the synthetic bone. In the human bones the CaS/HA was not able to spread around the screws properly and did not increase the stability of the screw.

To improve our knowledge about the mechanical properties of CaS/HA and bone, a study was conducted using 3D imaging at synchrotron facilities. In this thesis, 3D images of trabecular bone cores and CaS/HA specimens (millimetres) were acquired at high speed (seconds) and high resolution (micrometres), while loading the specimens. The images were used to show how damage initiates and progresses differently in bone and CaS/HA. The specimens with bone and CaS/HA combined revealed that the CaS/HA protects and strengthens the bone.

The computer models presented in this study accurately described the mechanical behaviour of the hip under loading. This can aid further development of this type of models to predict a patient's risk for a hip fracture. These models have also shown that CaS/HA is a useful bone cement that can increase hip strength, thus helping to prevent fractures. The added knowledge that CaS/HA strengthens and protects the bone from damage can help to find more clinical applications for this material, such as improving fracture fixation with dynamic hip screws.

# Populärvetenskaplig sammanfattning

Världens befolkning åldras. Hos äldre personer minskar bentätheten gradvis och hos kvinnor går processen snabbare efter klimakteriet. Låg bentäthet medför en ökad risk för höftfrakturer, vilket innebär att fler och fler människor bryter framförallt lårbenshalsen . För att minska antalet frakturer är det viktigt att patienter med hög risk identifieras innan de får sin första fraktur. Idag bedöms risken med hjälp av en bentäthetsmätning utifrån en röntgenbild i 2D. Arbetet i den här avhandlingen utgår från hypotesen att en bättre riskbedömning kan göras baserat på benstyrka som beräknas med datormodeller i 3D. Ett av målen i avhandlingen är att utveckla datormodeller och validera dem mot experiment där mekanisk prövning av lårben genomförts för att efterlikna ett fall åt sidan.

En patient som bedöms ha hög risk för fraktur behandlas med läkemedel som förhindrar att bentätheten minskar ytterligare. Läkemedlen är effektiva men har begränsad förmåga att främja ny benbildning. Läkare använder bencement för att till exempel stabilisera implantat och stärka hoptryckta ryggkotor, men bencement har ännu inte använts för att stärka ben i höften. Kalciumsulfat/hydroxiapatit (CaS/HA) är en typ av bencement som liknar benvävnad. Materialet har redan använts i flera ortopediska tillämpningar som har visat hur kroppen kan bryta ner cementet och ombilda det till ny benvävnad. De mekaniska egenskaperna behöver dock kartläggas mer i detalj. Patienter som får en höftfraktur till följd av låg bentäthet får ofta en höftledsprotes. Ett annat alternativ är att fixera frakturen med hjälp en dynamisk höftskruv som sammanfogar och stabiliserar de olika delarna. Dessa skruvar lossnar lätt i patienter med låg bentäthet och då kan bencement användas för att stabilisera skruven. Ett mål i den här avhandlingen är att undersöka hur CaS/HA kan användas på ett effektivt sätt i kliniken för att förhindra och behandla höftfrakturer.

Den här avhandlingen inleds med en undersökning av höftens mekaniska egenskaper. Lårben från avlidna donatorer belastades till fraktur i en uppställning som efterliknade ett fall åt sidan. Höghastighetskameror användes

för att noggrant mäta hur benen deformerades under belastningen. Efter de mekaniska testerna skapades datormodeller i 3D av benen. Modellerna baserades antingen på kliniska CT-bilder eller mikro-CT-bilder med högre upplösning. Modellerna som baserades på kliniska CT-bilder kunde förutspå var och vid vilken belastning benbrotten skedde. Modellerna kunde även beskriva deformationen med hög noggrannhet, dock något sämre i områden där benen hade en ojämn yta. Med mikro-CT-modellerna kunde benens yta modelleras med större noggrannhet och även inkludera ojämnheter på ytan. Resultaten från dessa modeller visade att lokala deformationer påverkas av ojämnheter på benets yta.

Avhandlingen fortsätter med en undersökning av kliniska användningsområden för CaS/HA. Datormodeller i 3D användes för att visa hur injektioner av CaS/HA kan förstärka lårbenshalsen. Hur mycket starkare benen blev berodde främst på var den simulerade injektionen av CaS/HA placerades. Dessutom gjordes mekaniska tester för att undersöka om en dynamisk höftskruv kunde stabiliseras med hjälp av en injektion av CaS/HA vid skruvens spets. Undersökningen gjordes genom att fästa skruvar med och utan CaS/HA i syntetiskt och humant ben. Genom att mäta vilken kraft som behövdes för att dra ut skruvarna ur benet visade det sig att CaS/HA hjälpte till att stabilisera skruvarna i det syntetiska benet. I det humana benet kunde inte CaS/HA spridas tillräckligt runt skruven och därför fanns inte heller någon tydlig stabiliserande effekt.

För att förbättra datormodellerna med CaS/HA och ben undersöktes de mekaniska egenskaperna hos CaS/HA ytterligare med hjälp av avbildning i 3D på synkrotronanläggningar. Små prover (millimeter) avbildades i 3D med hög hastighet (sekunder) och med hög upplösning (mikrometer) samtidigt som proverna belastades. Bildernas användes för att visa att skador uppstår och sprider sig olika i benvävnad och CaS/HA. Prover med både ben och CaS/HA visade att CaS/HA skyddar och stärker benvävnaden.

Datormodellerna i den här studien kan beskriva höftens mekaniska egenskaper under belastning noggrant. De kan därför bidra till utvecklingen av den här typen av modeller för att förutspå frakturrisk hos patienter. Modellerna har också visat att CaS/HA är ett användbart bencement som ökar benstyrkan och därmed förhindrar frakturer. CaS/HA kan också användas i kombination med dynamiska höftskruvar för att förbättra frakturfixering. Den nya kunskapen att CaS/HA stärker och skyddar benvävnad från skador kan bidra till att utforska nya användningsområden för materialet och driva utvecklingen så att behandlingen prövas på patienter.

# Abstract

Due to the aging population, hip fracture incidence has been increasing over the past decades. Measurements of bone mineral density with dual energy X-ray absorptiometry are the gold standard for hip fracture risk assessment, where patients with a low bone density have a high risk of fracture. However, many people that are not diagnosed to be at risk, still fracture their hip. Calculations of bone strength using subject-specific finite element (FE) models, can improve fracture risk prediction, but further improvement is required.

Patients with a high fracture risk are often prescribed pharmaceutical treatment in order to increase bone density systemically. As systemic response to treatment is limited, other options to prevent fractures by improving the bone strength are investigated. One of those options is the injection of biomaterials in the femoral neck. In case of a hip fracture due to a low-energy fall, total hip replacement is generally preferred over joint-preserving methods like fixation using a dynamic hip screw. Screw fixation comes with a risk of screw instability, especially in low-density bone. Bone cements can be used to improve fixation of orthopaedic implants and fracture fixation devices. Calcium sulphate/hydroxyapatite (CaS/HA) is an injectable biomaterial that has been used, for example, to reinforce collapsed vertebrae and to stabilize wrist fractures.

The work presented in the thesis aims to improve fracture risk prediction, and fracture prevention and repair methods with use of CaS/HA. This is achieved through a combination of experimental mechanical tests at organ and tissue scale, and development and thorough validation of FE models of the proximal femur.

In the first part of this thesis, 12 cadaveric femora were used in an experiment where the bones were loaded until fracture in a configuration developed to replicate a fall to the side. During loading, high-speed cameras were used to image both the medial and lateral side of the femoral neck allowing for full-field strain measurements using digital image correlation. The femora were imaged with clinical CT before and micro-CT before and after mechanical testing. Using the acquired CT images, FE models were developed at two different resolutions to determine their ability to capture the fracture force, fracture location and surface strains. The FE models based on the clinical CT

images were able to accurately capture the fracture force and identify regions where the bone would fracture. These models could also capture the strains with high accuracy. However, the strains were not predicted as accurately in regions with high surface irregularity. The models based on the micro-CT images could show, with higher accuracy, how the strains were distributed around local porosity (e.g., due to vascularization) in the femoral neck and how these influenced the fracture pattern.

The thesis continues with an investigation of fracture prevention and repair methods through the use of CaS/HA. The ability of CaS/HA to increase the fracture strength of the proximal femur for fracture prevention and its ability to stabilize a dynamic hip screw used for fracture repair was investigated. The increase in fracture strength was investigated using FE models. These models showed that CaS/HA can increase the fracture strength of the femur approximately 20% when injected close to the cortex in the lateral neck. Pullout tests using a dynamic hip screw were performed on synthetic bone blocks and femoral heads from hip fracture patients. In the synthetic blocks, CaS/HA significantly increased the pullout strength. However, in the human bone the stability of the screw was not improved, because the cement could not easily spread into the threads of the screws. The mechanical behaviour of CaS/HA and bone was further investigated using high-resolution synchrotron X-ray tomography. Cylindrical trabecular bone specimens with and without CaS/HA were imaged with tomography during in-situ loading of the samples. The images revealed that CaS/HA reinforced the bone, and that CaS/HA is a brittle material that will crack before the bone.

To conclude, in this thesis FE models are presented showing accurate prediction of fracture strength, which can be used for improved fracture risk assessments. Furthermore, the work provides insight in how CaS/HA behaves mechanically and how it can be used to increase the fracture strength and to stabilize fixation devices in the femur. These insights can help to improve fracture prevention and fracture repair methods.

# List of appended papers

This thesis consists of a review of the author's work in the field of biomedical engineering. The following selection of the author's publications is referred to in the text by their Roman numerals. Papers I-VI are appended at the end of the thesis and have been reproduced with the permission of the copyright holders.

I. Grassi, L., **Kok, J.**, Gustafsson, A., Zheng, Y., Väänänen, S.P., Jurvelin, J.S., Isaksson, H. Elucidating failure mechanisms in human femurs during a fall to the side using bilateral digital image correlation. *Journal of Biomechanics (2020)*. 106, 109826.

II. **Kok, J.**, Grassi, L., Gustafsson, A., Isaksson, H. Femoral strength and strains in sideways fall: validation of finite element models against bilateral strain measurements. *Journal of Biomechanics (2021)*. 122, 110445.

III. **Kok, J.**, Odin, K., Rokkones, S., Grassi, L., Isaksson, H. Accounting for foramina in finite element models of the femur affects strain prediction. *Manuscript under preparation*

IV. **Kok, J.**, Širka, A., Grassi, L., Raina, D.B., Tarasevičius, Š., Tägil, M., Lidgren, L., Isaksson, H. Fracture strength of the proximal femur injected with a calcium sulfate/hydroxyapatite bone substitute. *Clinical Biomechanics (2019)* 63, 172–178.

V. **Kok, J.**, Širka, A., Liu, Y., Tarasevičius, Š., Belickas, J., Tägil, M., Lidgren, L., Isaksson, H., Raina, D.B. Augmenting a dynamic hip screw with a calcium sulfate/hydroxyapatite biomaterial. *Medical Engineering and Physics (2021)* 92, 102-109

VI. **Kok, J.**, Törnquist, E., Raina, D.B., Le Cann, S., Novak, V., Širka, A., Lidgren, L., Grassi, L., Isaksson, H. Fracture behavior of a composite of bone and calcium sulfate/hydroxyapatite. *Manuscript submitted*

In paper I, the author of this thesis largely performed the data processing for the digital image correlation. The author of this thesis also aided in the sample preparation and experiment. In papers II-VI, the author of this thesis planned the studies together with the co-authors, developed the experimental and numerical methods and was the main responsible for writing the manuscripts.

# Acknowledgements

These past years have been a wonderful journey. I've met many interesting people and have made new friendships that I know will last a lifetime.

The first people that I would like to thank are the people that have made my PhD possible, my supervisors, Hanna and Lorenzo. Hanna, thank you for guiding me through all steps of my studies and teaching me how to become an independent researcher. Lorenzo, thank you for all your help. Not only have you given me feedback on all sorts of manuscripts, abstracts, and other documents, you've also made me better understand what the research world is like and what the life of a researcher can be.

I would like to thank my opponent, Harry van Lenthe, and the members of the examination committee, Svein Kleiven, Cecilia Persson, Björn Rosengren, Christina Bjerkén, and Dmytro Orlov, for critically reading my thesis to ensure the quality of my work.

To all my colleagues in the biomechanics group, thank you all for all the great moments we've had throughout the years. I've felt at home from the first day I started and that has not gone away. Thomas, you finished only a few months before me, but I already miss you around the office. Thank you for the fun days and evenings. All the conversations we've had, fun and serious, have really meant a lot to me. Anna, thank you for being the best office mate a person could wish for. Isabella, Elin, Maria, thank you for the fun AWs and for being all-round great colleagues. Gustavo, thank you for the enjoyable days at the BioMEP seminars. Tobias, Kunal, Hector, welcome to the group.

To everybody in the Orthopaedics group and from Kaunas, thank you for keeping my research close to the clinics. Deepak, from my first year we've started collaborating. I have enjoyed every second of it and hope we will be able to continue this in the future. Aurimas and Sarunas, thank you for your hospitality in Kaunas. Lars and Magnus, thank you for all your valuable input and help. Yang and Sujeesh, thank you for your help and always kindly welcoming me at C12.

To all the colleagues and students that have come and gone over the years. Hannicka, Mikael, and Sophie, it has been great working with you, talking science with you, and having beers with you. Catrin, Karin, Sofia, Nils, Ornella,

it has been a pleasure supervising you. I've learned a lot from all of you. All other master students that have come by, thank you for keeping our group young and lively.

To all other colleagues at BMC and the E-house. Jonatan, William, Moritz, thank you for all the wonderful evenings and occasional lunches. We should have more barbecues and board game nights. Everybody at BMC, thank you for the fikas and the semla tastings. Johan, thank you for being a wonderful and open head of department. Ammi, Desiree, and Ulrika, thank you for all your patience and making my life a lot easier. I would also like to thank all the fierce competitors that have joined for the innebandy games throughout the years.

To all the people at BioMEP, thank you for the fun and educational seminars.

To Vladimir, thank you for all your help and patience during and after our imaging times at TOMCAT.

To all the people from Nayan, thank you for all the great practices, tournaments, and parties. I would like to give some special thanks to Kalle, for giving me a place to live for a while, for the great friendship outside of Nayan, and for really keeping the club alive.

To Ann-Mari Sellerberg Persson, thank you for putting a roof over my head. You are the best landlady a person could wish for.

To everybody from Drago, thank you for being the best. Even when living 1000 km apart, it is clear that our bond will last a lifetime. Our summer vacations have been loads of fun and helped me relax and reset my mind.

Aan mijn familie. Pap, mam, bedankt voor al jullie onvoorwaardelijke steun. Het is een hele reis geweest en ik kijk ernaar uit om weer dichter bij jullie te zijn. Anna, Lena, jullie zijn de beste zussen die iemand zich maar kan wensen. Onze tripjes naar Budapest en Athene hebben een goede trend gezet en hebben mij veel rust gegeven tussen al het werken.

Floor, mijn schat, we hebben elkaar in Wenen gevonden en sindsdien hebben we elkaar niet meer losgelaten. Bedankt dat je bereid was om voor mij naar Zweden te verhuizen. In deze toch moeilijke tijden heb jij mijn leven flink opgefleurd. Daarnaast wil ik graag de rest van de familie Akkermans bedanken voor alle gastvrijheid en gezelligheid.

Finally, I would like to thank all bodies that helped make my research possible: The Swedish foundation for strategic research (IB2013-0021), the Swedish Agency for Innovation Systems (VINNOVA) (2017-00269), the Swedish Research Council (2015-04795; 2019-04517), the European Union’s Horizon 2020 research and innovation program under the Marie Skłodowska-Curie grant agreement (713645), and the Birgit and Hellmuth Hertz' Foundation.

# List of abbreviations

| | |
|---|---|
| **µCT** | micro X-ray computed tomography |
| **aBMD** | areal bone mineral density |
| **BgV/TV** | background volume / total volume |
| **BMD** | bone mineral density |
| **BV/TV** | bone volume / total volume |
| **CaP** | calcium phosphate |
| **CaS** | calcium sulphate |
| **CaS/HA** | calcium sulphate/hydroxyapatite |
| **CT** | X-ray computed tomography |
| **CV/TV** | calcium sulphate hydroxyapatite volume / total volume |
| **DHS** | dynamic hip screw |
| **DIC** | digital image correlation |
| **DVC** | digital volume correlation |
| **DXA** | dual energy X-ray absorptiometry |
| **FE** | finite element |
| **FRAX** | fracture risk assessment tool |
| **HA** | hydroxyapatite |
| **PMMA** | polymethylmethacrylate |
| **QALY** | quality adjusted life year |
| **ROI** | region of interest |
| **THR** | total hip replacement |
| **WHO** | world health organization |

# Table of Contents

**Popular science summary** ..... **vii**

**Populärvetenskaplig sammanfattning** ..... **ix**

**Abstract** ..... **xi**

**List of appended papers** ..... **xiii**

**Acknowledgements** ..... **xiv**

**List of abbreviations** ..... **xvi**

**1. Introduction** ..... **1**

**2. Aim and design of the study** ..... **3**

2.1. Design of the study ..... 4

**3. Background** ..... **5**

3.1. Hip Fractures ..... 5

Fracture risk prediction ..... 8

Fracture prevention ..... 8

Fracture repair ..... 9

3.2. Biomaterials ..... 9

3.3. X-ray tomography imaging techniques ..... 11

Clinical CT ..... 11

Micro-CT (µCT) ..... 12

Synchrotron CT ..... 12

3.4. Mechanical testing ..... 13

Organ scale mechanical testing ..... 14

Mechanical testing of (fracture) fixation devices ..... 15

Tissue characterization ..... 16

Digital image correlation ..... 17

Digital volume correlation ..... 19

3.5. Finite element models ..... 20

**4. Material & Methods** ..... **23**

4.1. Sideways fall, mechanical testing and FE modelling (Study I, II, III) ..... 23
Subjects and imaging ..... 23
Mechanical testing (study I) ..... 24
FE analysis (study II, III) ..... 26
Data analysis ..... 28
4.2. Fracture strength after CaS/HA injection (study IV) ..... 29
Subjects and imaging ..... 29
FE and data analysis ..... 31
4.3. Screw pullout strength with CaS/HA (study V) ..... 33
Specimens and imaging ..... 33
Mechanical testing ..... 35
Data analysis ..... 37
4.4. Bone-CaS/HA mechanical behaviour (study VI) ..... 37
Specimens, imaging, and mechanical testing ..... 37
Data analysis ..... 38

**5. Results ..... 40**
Sideways fall mechanical testing (study I) ..... 40
Sideways fall FE modelling (study II, III) ..... 42
Fracture strength after CaS/HA injection (study IV) ..... 44
Screw pullout strength with CaS/HA (study V) ..... 46
Bone-CaS/HA mechanical behaviour (study VI) ..... 48

**6. Discussion ..... 50**
6.1. General ..... 50
Sideways fall mechanical testing ..... 50
FE modelling ..... 51
Screw pullout strength with CaS/HA ..... 53
In situ loading ..... 55
6.2. Limitations ..... 56
Mechanical testing ..... 56
FE modelling ..... 58
6.3. Future perspective ..... 59
Further model development and validation ..... 59
Toward clinical application ..... 61

**7. Summary and conclusions ..... 63**

**8. References ..... 65**

**Appended papers ..... Error! Bookmark not defined.**

# 1. Introduction

Hip fractures are a growing socio-economic problem world-wide. In the EU, 610 000 fractures were recorded in 2010 and 810 000 fractures are expected in 2025 (Hernlund et al., 2013). The main cause for the increase in fracture incidence is the aging of the population. Increasing age and a declining bone density increases the risk of fracture. Caucasian women have a lifetime risk of fracture of 16-18% and for men this risk is 5-6% (Kannus et al., 1996). Of these fractures, the majority is the result of a low-impact fall to the side (Parkkari et al., 1999). After a sustained fracture, the choice for surgical repair is often total hip arthroplasty. This is commonly followed by long periods of immobilization (Ekström et al., 2009). Together this leads to estimated costs of over €20 billion and a loss of approximately 600.000 Quality Adjusted Life Years per year in the EU (Hernlund et al., 2013). There is a clear need for improved fracture risk assessment, prevention, and repair methods.

Today, risk of fracture is directly assessed through bone density measurements using dual X-ray absorptiometry. The world health organization (WHO) defines osteoporosis as a bone density 2.5 standard deviations below that of healthy young people of the same sex and population (WHO, 1994). Approximately 3 out of 4 people that fracture their hip would not be osteoporotic per this definition (Pasco et al., 2006). Some improvement can be achieved through the inclusion of epidemiological parameters through, for example, FRAX (Kanis et al., 2009). Still, these methods do not account for local weaknesses in the bone. Further improvement in predicting the fracture risk can be achieved using 3D subject-specific finite element (FE) models (Orwoll et al., 2009; Enns-Bray et al., 2019). These models can account for more details in the femur's geometry and density to predict the strength required for it to fracture. Validation against experimental measurements of force, fracture location, and strain can ensure that these models accurately represent the mechanical behaviour of bone.

People that have been assessed to be at high risk of fracture are prescribed a pharmaceutical treatment and should receive dietary advice and are recommended physical exercise. Through these methods, further loss of bone can be limited and bone density can potentially even increase somewhat.

However, the efficacy of the treatments has been debated (Järvinen et al., 2015) and less than half of the fractures are prevented (Barrionuevo et al., 2019).

Augmentation of a bone through injection of a biomaterial can be used to strengthen the bone. In vertebrae, bone cements are used to stabilize the vertebrae and reduce pain after a compressive fracture (i.e., vertebroplasty) (Levy et al., 2012). In hips, injection of a bone cement in a non-fractured hip (i.e., femoroplasty) can increase the fracture strength of the hip (Heini et al., 2004). This is currently not clinically applied because the most used bone cement, PMMA, can have adverse effects including osteonecrosis from heating during setting and stress-shielding due to the high stiffness of PMMA. There is also a big ethical question surrounding the injection of bone cement into non-fractured bone (Varga et al., 2016).

In young healthy people that suffer from a hip fracture, the preferred treatment is fixation using a dynamic hip screw (DHS) (Lowe et al., 2010). This screw connects the two halves of the femur, while still allowing the two parts to be pressed together, leading to a more natural healing and preserving the hip joint (Lowe et al., 2010). In patients with low bone density, a DHS is not the first choice because there is an increased risk of screw instability. Similar to increasing the fracture strength of a femur through femoroplasty, bone cements have the ability to limit migration of orthopaedic implants.

Experimental and numerical biomechanical studies can be used to improve and evaluate techniques for fracture strength predictions, fracture prevention and repair. To improve fracture strength predictions, full-field strain measurements using digital image correlation (DIC) can be used on bone for validation and development of FE models (Grassi et al., 2016). Similar FE models can be used to investigate the effect of bone cements on the mechanics of the femur. Resorbable cements are gaining interest because they can overcome issues present in traditional cements such as heating and stress shielding (Tan et al., 2013). New applications and the detailed mechanical behaviour of these cements are continuously investigated and seem promising.

# 2. Aim and design of the study

The overall aim of the presented thesis work was to investigate new fracture strength prediction tools, and fracture prevention and repair methods. A combination of experimental and numerical studies was performed for the validation of finite element models and investigation of orthopaedic applications of a bone cement based on calcium sulphate/hydroxyapatite (CaS/HA).

The aims of the individual studies were:

I) To gain insight in the mechanical behaviour of the human femur under sideways fall loading using high-speed bilateral 3D digital image correlation measurements.

II) To validate a finite element model of the proximal femur under sideways fall loading using bilateral 3D digital image correlation measurements.

III) To determine the influence of surface irregularity in the femoral neck on local strain distributions and fracture location for a femur in sideways fall using high-resolution finite element models.

IV) To investigate the feasibility of injecting CaS/HA in the femoral neck in a clinical setting and calculate the potential fracture strength increase using finite element models.

V) To determine whether an injection of CaS/HA can improve the primary fixation of a dynamic hip screw.

VI) To determine if and how bone augmentation with CaS/HA alters the fracture behaviour of bone.

## 2.1. Design of the study

The specific aims of the individual studies are visualized as the design of the study in figure 2.1.

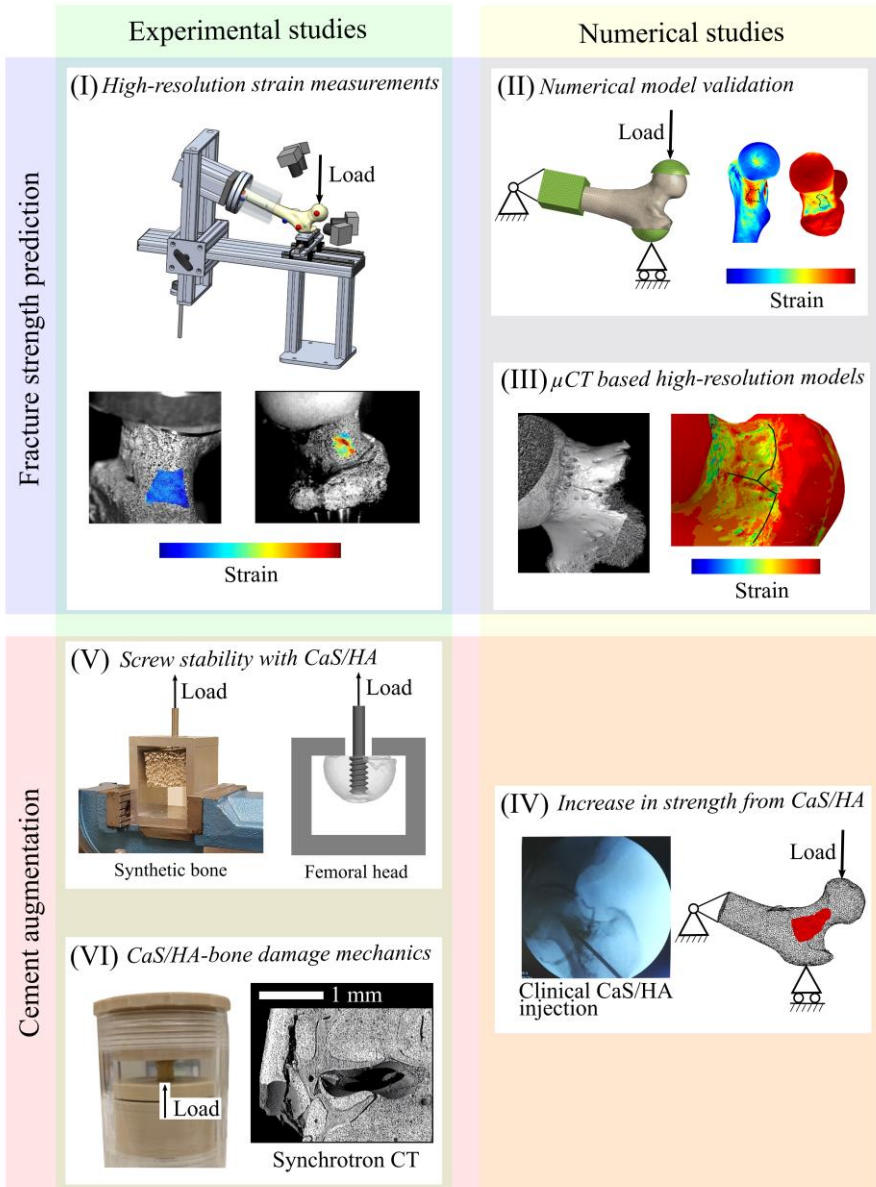


*Figure 2.1. Overview of the design of the study. The roman numerals (I-VI) refer to the aims and appended studies.*

# 3. Background

## 3.1. Hip Fractures

Osteoporosis is a condition that is represented by skeletal fragility and an increased fracture risk. This fragility originates mostly from a reduction in bone mass and bone quality due to aging. Osteoporotic bone is weak enough to fracture under low loads (i.e., loads that the body is typically exposed to during daily routines) (Dempster et al., 2021). Following the world health organization (WHO) guidelines, osteoporosis is diagnosed through measuring the areal bone mineral density (aBMD). The most used technique for measuring aBMD is dual energy X-ray absorptiometry (DXA). A patient is diagnosed with osteoporosis when their measured aBMD values fall 2.5 standard deviations below that of an average set of healthy young people of the same sex and population (WHO, 1994).

The main building blocks relevant to the mechanics of bone are inorganic minerals in the form of hydroxyapatite, organic collagen fibrils, and water. These building blocks are arranged in different ways across various hierarchical levels (Reznikov et al., 2018). At the nanoscale, soft collagen fibrils are connected through enzymatic cross-links (Burr, 2019). Between the collagen fibrils stiff hydroxyapatite mineral crystals are deposited. Water can be found between and inside the collagen and mineral. At a larger scale these mineralized fibrils form lamellar sheets that are the basis of both the trabecular and cortical bone.

Long bones, such as the femur (thighbone), consist of two types of bone, a dense cortical bone shell (thickness ~0.1-10 mm) and porous trabecular bone (thickness ~0.1-0.4 mm) where the remaining space is filled with bone marrow. Blood and nutrients are supplied through foramina (~0.5-1.5 mm) in the cortical shell (Mei et al., 2019). This supply allows bone to constantly renew and remodel itself. The remodelling includes resorption of old bone and formation of new bone. The remodelling balance is dependent on the mechanical loads to which bone is exposed. This way an optimal structure for carrying loads is created (Wolff, 1870). This means that bone is denser in regions where it is exposed to high loads. Additionally, in regions where loading is highly directional (e.g., the proximal femur), bone is highly anisotropic. These

adaptations also mean that bone behaves differently depending on the loading direction. During aging a clear reduction in the bone density in the proximal part of the femur can be seen (Figure 3.1). When the bone breaks in this region it is classified as a hip fracture. These fractures are divided into sub-categories. The most common types of hip fracture in patients with osteoporosis are cervical and intertrochanteric fractures (Figure 3.1) (Fox et al., 1999).

Low-energy falls are the main cause for hip fractures in osteoporotic patients (Parkkari et al., 1999; Berry and Miller, 2008; Geusens et al., 2003; Harvey et al., 2016). During aging, fall incidence gradually increases due to a reduction of motor control (Shumway-Cook et al., 1997). For each type of fall, the risk of fracture is different. A fall to the side is most associated with a high risk for a hip fracture (Greenspan et al., 1998). These falls can occur during normal daily activities, such as standing up or turning around.

Due to aging of the population, the socio-economic impact of hip fractures has increased over the past decades (Hernlund et al., 2013; Borgström et al., 2020). This impact comes from an accumulation of high incidence, disability following hip fracture, and mortality:

- Incidence, in the EU, is estimated to increase from 610 000 in 2010 to 810 000 in 2025 (Hernlund et al., 2013). Once someone has suffered a hip fracture, the 10-year risk of fracturing the other hip increases to 30-35% (Sobolev et al., 2015).
- Disability following a hip fracture is high. Only 40-60% of people recover to pre-fracture levels of mobility (Dyer et al., 2016). These numbers are even worse for long-term nursing home residents, where only 1 in 5 regains pre-fracture mobility (Neuman et al., 2014).
- Mortality within one year of the first hip fracture is approximately 16%. After a second hip fracture, the mortality within one year increases to 24% (Berry et al., 2007).

Altogether, in the EU, this has led to a loss of approximately 600 000 Quality Adjusted Life Years (QALYs) in 2010 (Hernlund et al., 2013). Not accounting for the lost QALYs, the associated costs were approximately €20 billion. Including the lost QALYs in the cost estimates, costs were estimated to exceed €50 billion.

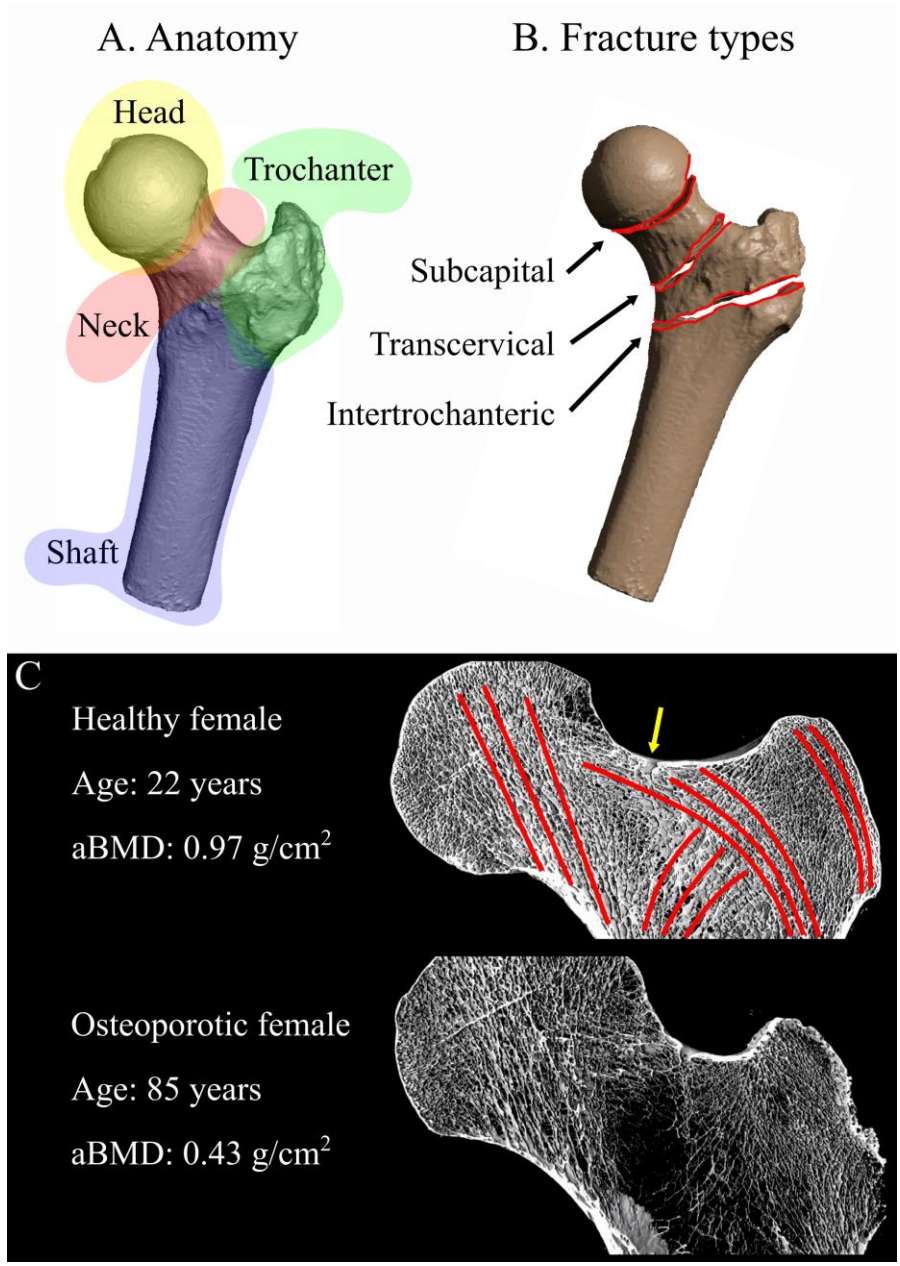


*Figure 3.1. A) A proximal femur with anatomical locations. B) Three of the most common hip fracture types. C) Cross-sections (~2.5 mm) of a healthy and an osteoporotic proximal femur. The red lines indicate the main orientation of the trabecular bone. The yellow arrow indicates a foramen in the cortical shell through which a blood vessel enters the bone.*

## Fracture risk prediction

The risk of fracture is often predicted from aBMD measurements. Several studies have shown that 50-75% of patients that suffered a hip fracture would not be classified as osteoporotic based only on their aBMD values (Sandhu et al., 2010; Pasco et al., 2006). To improve risk assessment based on aBMD measurements, epidemiological risk factors can be included. Risk factors include low BMI, prior fractures, parental history of fractures, smoking, long-term use of glucocorticoids, rheumathoid arthritis, and high alcohol consumption (Kanis et al., 2018).

Several tools that can estimate the fracture risk with or without aBMD measurements have been developed. The Fracture Risk Assessment Tool (FRAX) is a widespread clinical tool that is mainly used for long-term (5- or 10-year) fracture risk predictions (www.shef.ac.uk/FRAX/) (Kanis et al., 2009). Although the use of these algorithms generally leads to an improvement, the predictive capabilities are still limited. One reason is that it typically does not account for factors such as the shape of bones, or patient-specific risk of falling, which are also heavily associated with increased fracture risk (Viceconti et al., 2015). Finite element (FE) models can account for the complex structure and local variations in bone mineral density (more in section 3.5). With these models a patient-specific fracture strength of the femur can be calculated. The fracture strength is a strong predictor for fracture risk (Orwoll et al., 2009; Enns-Bray et al., 2019).

## Fracture prevention

Patients with a high fracture risk can be treated in multiple ways, depending on factors such as age, sex, and severity of osteoporosis. In most cases, some form of pharmacological treatment is prescribed (McCloskey et al., 2021). Currently, the most commonly prescribed drugs are oral bisphosphonates. Bisphosphonates are incorporated in the bone and inhibit the resorption of bone. They have been shown to reduce hip fracture risk about 30-40% (Barrionuevo et al., 2019). Additionally, bisphosphonate incorporation in bone is not reversed when quitting the treatment. This means that the reduction in fracture risk is somewhat maintained, after treatment is stopped. However, an adverse effect is that prolonged treatment increases the risk for atypical femoral fractures or osteonecrosis of the jaw (Saita et al., 2015; Jha et al., 2015). After bisphosphonates, treatment with denosumab is the most prescribed (McCloskey et al., 2021). Denosumab is another antiresorptive drug that has been shown to reduce hip fracture risk with 40% within 3 years, when administered subcutaneously twice per year (Cummings et al., 2009). Stopping this treatment reverses the positive effects and results in rapid bone loss (McClung et al.,

2017). It is therefore recommended that treatment with denosumab is followed by other treatment for osteoporosis. It has been argued that for patients already at high risk, pharmacological treatment may not be sufficient (Järvinen et al., 2015), partially due to a delayed response to the therapy (Ferrari et al., 2016).

In addition to pharmacological treatment, patients often receive nutritional advice and physical therapy. Calcium and vitamin D are associated with good bone health and supplements are generally prescribed together with pharmacological treatment (Mendes and Sahni, 2021; McCloskey et al., 2021). Physical therapy can help patients regain musculoskeletal control and improve coordination, which prevents them from falling (Kontulainen and Johnston, 2021). However, sustained bone strength is most affected by physical activity during puberty and adolescence (Faulkner and Bailey, 2007; Karlsson and Rosengren, 2020).

### Fracture repair

After a fragility fracture, surgery to either stabilize or replace the hip joint is often the best option. Sub-capital fractures, that are not displaced, can in some cases be left untreated. However, in 79% of patients with this type of fracture, the femoral head would still end up displaced without surgery (Bukata et al., 2021).

One option for surgical treatment in non-displaced fractures is internal fixation using orthopaedic devices. This type of surgery is often preferred because it allows preservation of the hip joint (Lowe et al., 2010). A device commonly used for internal fixation is a cannulated dynamic hip screw with a side-plate. However, any type of fixation surgery in patients with low bone density carries a risk of complications (von Rüden and Augat, 2016). Common complications are penetration of the screw through the femoral head and extensive distal sliding of the screw (Jiang et al., 2015). These complications led to reoperation rates of 8-19% and 8-16% were converted to hip arthroplasty (Oñativia et al., 2018). Patients with low bone density or displaced fractures, therefore, typically receive a partial or total hip replacement (Lowe et al., 2010).

## 3.2. Biomaterials

Biomaterials can be used as a scaffold for formation of new tissues, or as a system for drug delivery (Burg et al., 2000). A good biomaterial for bone tissue engineering (Albrektsson and Johansson, 2001) has the following properties:

- Osteoinduction: the ability to induce formation of bone.

- Osteoconduction: allowing bone ingrowth or bone growth on the surface.
- Osseointegration: the ability to integrate well with the surrounding bone.

Biomaterials are made of different organic and inorganic bases, such as collagen, gelatine, hydroxyapatite, calcium phosphate, and metals.

To improve stabilization of fractures or implants, acrylic-based biomaterials are often used. These materials are also commonly called bone cements and are generally created by mixing a powder and a liquid which can be moulded or injected before it sets. Polymethylmethacrylate (PMMA) was the first cement used to improve the stability of a hip implant (Charnley, 1961). PMMA was later also used to stabilize internal fracture fixation (Harrington et al., 1976) and as means to reinforce collapsed vertebrae, i.e., vertebroplasty (Galibert et al., 1987). By injecting PMMA into the broken vertebra, the fracture was stabilized and pain reduced.

Although acrylic-based bone cements are biocompatible, they do not induce bone formation and are not resorbable. In the case of vertebroplasty, the lack of bone-ingrowth, in combination with the high stiffness of the cements, increases the risk of fracture in adjacent vertebrae. This has led to fracture rates after vertebroplasty that range from 20 to 60% (Lin et al., 2008a, 2008b). Additionally, the setting temperature of PMMA typically reaches over 70°C, which can result in local osteonecrosis (DiPisa et al., 1975).

Similar to vertebroplasty, bone cements have been investigated for augmenting the femoral neck through femoroplasty. The first studies conducted were mechanical tests where large volumes (28-41 ml) of PMMA were injected in the femoral neck (Heini et al., 2004). The outcome was that the force required to break the femur nearly doubled. However, the large injected volumes create a high risk of osteonecrosis due to the high setting temperature of PMMA. This temperature can be reduced by injected less material (~15 ml) (Sutter et al., 2010) or by incorporating glass ceramic particles (Beckmann et al., 2007). However, with these methods the achieved strength increases were either not significant (Sutter et al., 2010) or approximately 40% (Beckmann et al., 2007). Due to the risks and ethical questions surrounding prophylactic augmentation of the femur, clinical acceptance is still low (Varga et al., 2016).

Resorbable osteoinducing biomaterials have gained traction for orthopaedic use over the past decades. These materials often have a base of calcium sulphate (CaS) or calcium phosphate (CaP), that resorbs within weeks-months after the injection (Knaack et al., 1998; Wang et al., 2016). Hydroxyapatite (HA), the mineral building block of bone, can be mixed with CaS or CaP to provide a scaffold for bone ingrowth, leading to high osteoconductivity (Wang et al.,

2016). Due to the resorbable nature of these materials, they can also be injected in combination with drugs, like antibiotics or bone morphogenetic proteins (Raina et al. 2019; Stravinskas et al. 2018). These drugs are then slowly released during resorption of the cement, extending the time when the drugs are effective. Several studies have investigated the use of the CaS/HA mixture in vertebroplasty and for stabilizing wrist fractures (Nilsson et al., 2013; Abramo et al., 2010). This led to significant pain relief and increases in bone mineral density (Hatten and Voor, 2012).

## 3.3. X-ray tomography imaging techniques

X-ray computed tomography (CT) is a 3D imaging technique that can be used for the imaging of animals, patients, and non-living objects to visualize internal structures. An X-ray source generates X-rays with a specific intensity that is then measured with a detector plate to create an image. By placing a subject between the source and the detector the X-rays are attenuated and a decrease in intensity will be measured. Every material has a specific attenuation coefficient, which is strongly related to its density. By taking images from multiple angles, a 3D image volume can be reconstructed. The values assigned to each volume pixel (voxel) are largely related to the density of the imaged materials. This technique can be used at length scales varying from nanometres to metres.

To obtain quantitative measurements of the densities of the materials imaged, calibration phantoms can be included in the scans. When imaging bone, phantoms with materials with similar radiological density as bone (e.g., hydroxyapatite) are often used (Figure 3.2B). With the known densities, it is possible to calculate a relationship between the image intensity and the hydroxyapatite mineral density. This way the bone mineral density in each voxel can be approximated.

### Clinical CT

In a clinical setting, CT is used to support patient diagnostics (Figure 3.2A). In clinical scanners the X-ray source and the detector are rotated around the patient. Since long exposure to high energy X-rays can lead to tissue damage, the X-ray energy and scanning time are kept low. This leads to images that generally have a resolution around 1 mm and have relatively low contrast. With this type of CT, it is possible to obtain the 3D structure of a femur. However, smaller details, such as the trabecular structure (~150 μm), cannot be resolved.

With the use of a calibration phantom clinical CT scans can be used to determine the distribution of mineral density throughout the bone (Taddei et al., 2007). From the density mechanical properties can be derived to build accurate FE models (see section 3.5).

## Micro-CT (µCT)

Compared to clinical CT, µCT scanners are used to obtain images at a higher resolution (Figure 3.2C). There are two common variations in µCT scanners, small animal scanners for imaging of living animals such as mice or rats, and laboratory scanners used for imaging of non-living objects. Scanners for small animals use the same concept as clinical CT scanners but have a smaller field of view and can reach resolutions down to ~10 µm. In contrast, laboratory scanners are used for the imaging of non-living objects. Therefore, higher energies and exposure times up to several hours can be used. In this type of scanner, the sample rotates instead of the X-ray source and the detector, and resolutions down to ~1 µm can be reached.

At the higher resolutions achieved with µCT, trabecular structures of whole femora can be resolved (Figure 3.2C). This way, more detailed FE models can be built (Verhulp et al., 2006; Nawathe et al., 2014; Bahaloo et al., 2018). With these models it is possible to investigate the relationship between local microstructures and fracture events.

## Synchrotron CT

Synchrotron CT can reach resolutions similar to, and higher than, those reached by µCT scanners, while being at least hundred times faster (Figure 3.2D). This way, scanning times are reduced from hours to seconds. At synchrotron facilities, electrons are accelerated to speeds close to the speed of light. With use of magnetic fields in a ring of typically several hundreds of metres, the direction of the electrons is changed and large amounts of X-rays of a specific energy are emitted. As these facilities are very expensive, only a few dozen can be found around the world.

The rapid, high-resolution image acquisition with synchrotron CT can be used to load samples *in situ* (Singh et al., 2014). This way, damage propagating through, for example, samples of trabecular bone can be tracked (Turunen et al., 2020). With the use of digital volume correlation, it is also possible to obtain strain measurements at a sub-trabecular level (see section 3.4).

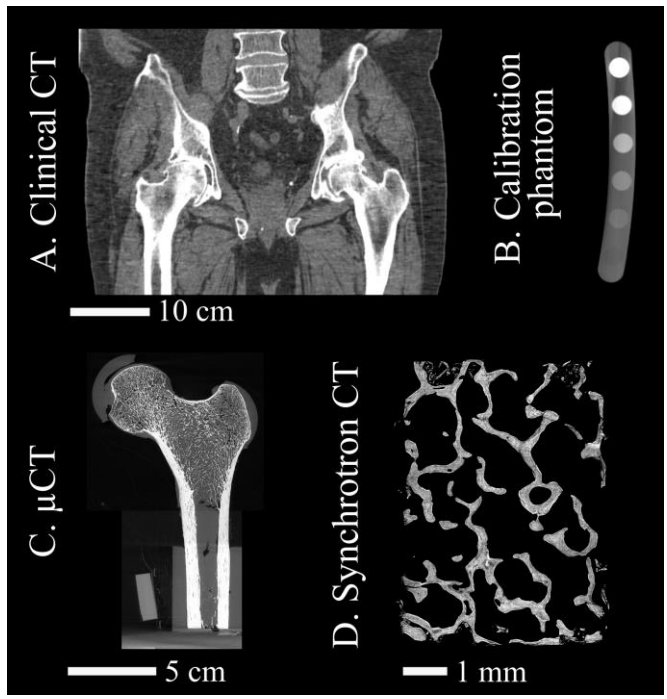


*Figure 3.2. A) Clinical CT image of a patient (voxel size: 1 mm, field of view: 500 x 500 x 329 mm$^3$, scanning time: 13 min). B) Clinical CT image of a calibration phantom with six rods with different hydroxyapatite densities. C) Laboratory µCT image of a cadaver proximal femur (voxel size: 57 µm, field of view: 67 x 103 x 173 mm$^3$, scanning time: ~2 hours). D) Synchrotron CT image of trabecular bone (voxel size: 2.75 µm, field of view: 11 x 11 x 3 mm$^3$, scanning time: 18 s).*

## 3.4. Mechanical testing

Mechanical testing can be used to characterize properties of bone and biomaterials at all length scales. At each length scale, the basis for mechanical testing is the application of a load or displacement on a specimen while recording both. From the resulting force-displacement curve, extrinsic mechanical parameters can be derived. When taking the shape of the specimen into account, a stress-strain curve can be calculated to obtain intrinsic material parameters (Reilly et al., 1974; Reilly and Burstein, 1975; Turner and Burr, 1993). Material parameters that are relevant for bone mechanics and often directly derived from these curves are:

- The yield and peak force.
- The yield and ultimate stress and strain.
- The stiffness or Young's modulus (i.e., the slope of the linear region).
- The work until peak force or failure (i.e., the area under the force-displacement curve).

By applying variations in the loading regime, more complex mechanical properties can be determined. For example, the mechanical behaviour of bone has been shown to depend on the loading rate (Carter and Hayes., 1976). At higher loading rates the stiffness of bone increases.

## Organ scale mechanical testing

On the organ scale bones vary greatly in shape, size, and density distribution. By carefully designing a setup for loading, many physiological or clinically relevant loading conditions can be replicated. In the case of the femur, the most commonly replicated loading conditions are:

- **Single-leg-stance:** A physiologically relevant loading condition, replicating a load to which the femur is exposed on a daily basis. The femur is typically constrained at its distal end and rotated to 8° adduction. The load is then applied on top of the femoral head (Figure 3.3A) (Cristofolini et al., 2007).
- **Sideways fall:** This loading condition is more clinically relevant, because it is more associated with hip fractures. The femur is typically placed sideways with an internal rotation of 15° and an adduction angle of 10° (Backman, 1957). The distal end is constrained to only allow rotation in the adduction/abduction directions. The greater trochanter is only constrained along the load axis and the load is applied to the femoral head (Figure 3.3B).

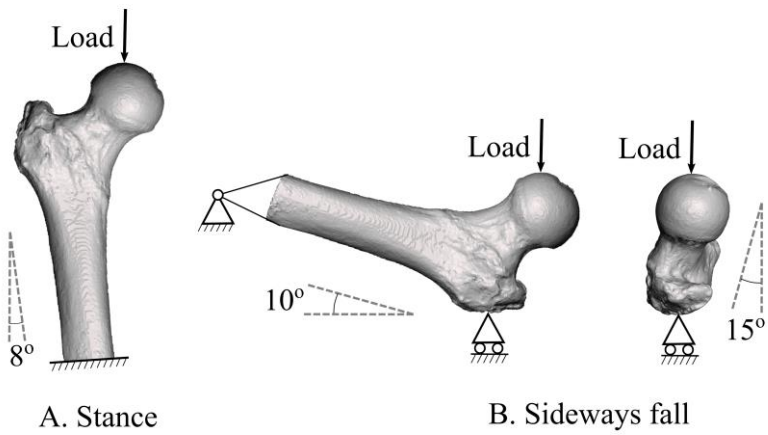


*Figure 3.3. Two loading conditions commonly used for ex vivo experimental testing of proximal femora. A) Single-leg-stance. B) Sideways fall.*

By loading until failure, the force and work required to fracture, and bone stiffness can be determined. Recordings of the experiment with high-speed cameras can be used to determine the location where damage initiates (Cristofolini et al., 2007). Strains on the surface of the bone can be measured in 3 dimensions at multiple locations with strain gauges. Zani et al. (2015) compared strains under stance and sideways fall loading conditions by applying strain gauges in 16 locations. Under stance loading, the highest tensile strains were measured on the superolateral side of the femoral neck. The highest recorded compressive strains were measured on the medial side. Under sideways fall, this was inverted, with high tensile strains on the medial side and high compressive strains on the superolateral side. The highest absolute strains were the compressive strains on the superolateral side under sideways fall. At this location fracture was initiated at forces ranging from 1.57 to 7.31 times the subjects their bodyweight.

## Mechanical testing of (fracture) fixation devices

Similar to organ scale mechanics special loading devices can be developed to test orthopaedic implants and fixation devices. Due to large biological variation when using animal or human cadaveric material, synthetic bone material is often used first to test new treatment options. In the case of surgical screws, one of the most common tests for comparison is a pullout test, where the screw is inserted in (synthetic) bone and pulled out. The main outcome in this kind of test is the peak force, but other relevant parameters are the stiffness, work, or the force at a specific displacement.

Eriksson et al. (2002) performed pullout tests on synthetic bone, where dynamic hip screws were augmented with PMMA or CaP cement. They concluded that PMMA significantly increased the pullout strength, whereas augmentation with a CaP cement even had a negative effect in higher density material, due to the need for predrilling. In human femoral heads, PMMA has been shown to be able to approximately double the pullout strength of a fixation device (Erhart et al., 2011). In other orthopaedic applications, augmentation with CaP based cements have shown significant increases in pullout strength. With augmentation of pedicle screws, increases in pullout strength of up to 73% have been recorded (Sun et al., 2020). In humeri and synthetic bone, suture anchors also reached approximately double the pullout strength through augmentation with a CaP cement (Diaz et al., 2020).

## Tissue characterization

To characterize the material properties of trabecular bone samples, mechanical compression testing is probably the simplest and most used approach. These tests can be done at various length scales but are generally performed on small (5-50 mm) cylindrical or cubic samples of trabecular or cortical bone. Compression is performed by applying a force or a displacement on the specimen, while recording changes in both parameters. Since these samples are small and have a known defined shape, the material properties can be assumed to be homogeneous and a stress-strain curve can be derived from the measured force and displacement. Due to the homogeneity of the samples, intrinsic material parameters can be obtained.

Early studies have shown the dependency of the compressive strength of bone on the apparent density and strain rate (Carter and Hayes, 1976). Similarly, the Young's modulus has been shown to be proportional to the strain rate to the power 0.06 (Carter and Hayes, 1977). The dependency of the Young's modulus is also largely dependent on the apparent density of the bone. Morgan et al. (2003) has shown that depending on the anatomic site the modulus-density relationship varies significantly. These variations are attributed to the large variation in trabecular structure. Although the ultimate stress and modulus of bone are related to the density of the bone, the yield and ultimate strain have been shown to be less dependent of these factors. Bone yields under a strain of approximately 1% (Bayraktar et al., 2004), and fails at a strain of 2-3% (Reilly et al., 1974).

## Digital image correlation

Digital image correlation (DIC) is a measurement technique that allows for full-field strain calculations (Sutton et al., 2009). This no-contact technique can be used as an alternative to strain gauges, of which only a few can be placed on the bone surface (Grassi and Isaksson, 2015). The basic idea is that multiple images are taken of a sample while it is loaded and that by matching subsets of the subsequent images, displacements are obtained (Figure 3.4). This way surface strains can be calculated at a higher spatial resolution.

DIC requires that the sample's surface includes many small unique details with high contrast. To achieve this, the surface of the sample is painted white and sprayed with black paint to create a random speckle pattern. During loading of the sample, multiple digital pictures are obtained. A region of interest is selected, and a grid of regularly spaced nodes is placed inside this region. For each node, a correlation window is defined in which a unique speckle pattern is found. In the subsequent image, a search window is defined in a region of the image that roughly matches the region of interest in the first image. A grid of nodes is placed also in this window. The correlation window from the first image is compared to equally sized selections around the nodes in the second image. The size of the search window should be as small as possible, but larger than the maximum local displacement between two images. For experimentally measured displacements, a confidence interval (σ) can be calculated as a measure for how accurately the displacement of each point is calculated between subsequent images (Sutton et al., 2009).

To obtain strains from the resulting displacement field the grid of nodes can, for example, be turned into triangles. This way a strain tensor can be calculated from the deformation gradient tensor **F**. The most commonly used strain tensor for DIC calculations is the Green-Lagrange strain tensor **E**, which is calculated as:

$$\boldsymbol{E} = \frac{\mathbf{1}}{\mathbf{2}}(\boldsymbol{F}^{\boldsymbol{T}}\boldsymbol{F} - \mathbf{I})$$

Where **I** is the unit tensor. To avoid incorrect strain calculations due to large rigid body rotations the engineering strains can be calculated. These can be calculated directly from the components of the Green-Lagrange strain tensor:

$$\varepsilon_{\boldsymbol{x}} = \sqrt{(\mathbf{1} + \mathbf{2}\boldsymbol{E}_{\boldsymbol{xx}})} - \mathbf{1}$$

$$\varepsilon_{\boldsymbol{y}} = \sqrt{(\mathbf{1} + \mathbf{2}\boldsymbol{E}_{\boldsymbol{yy}})} - \mathbf{1}$$

$$\varepsilon_{\boldsymbol{xy}} = \sin^{-1}\left(\frac{\mathbf{2}\boldsymbol{E}_{\boldsymbol{xy}}}{\sqrt{(\mathbf{1} + \mathbf{2}\boldsymbol{E}_{\boldsymbol{xx}})(\mathbf{1} + \mathbf{2}\boldsymbol{E}_{\boldsymbol{yy}})}}\right)$$

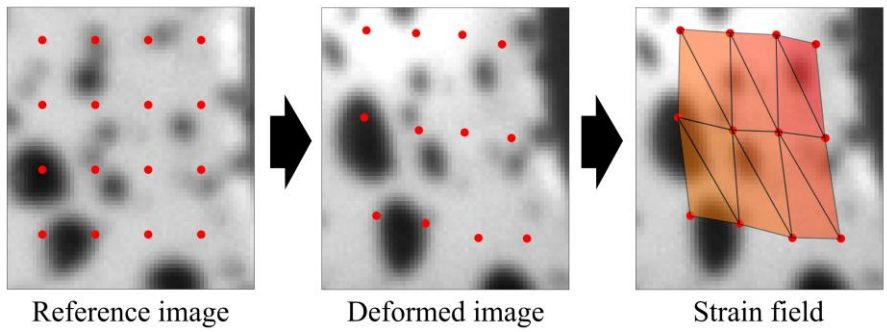


*Figure 3.4. The concept of digital image correlation. Regularly spaced nodes are placed on a reference image of the sample. Image subsets of the reference image are matched with subsets of the image of the deformed sample to measure displacements. From the displacements, strains are calculated to obtain a strain field.*

DIC was first used on human femora in 2011 (Op Den Buijs and Dragomir-Daescu, 2011). Femora were mechanically tested in a fall loading configuration at a displacement rate of 100 mm/s while being recorded with a high-speed camera (1024x512 pixels, 6000 frames per second). In this study, only a qualitative description of strains was given. Since then, more detailed DIC measurements have been performed. For example, Gilchrist et al. (2013) showed that DIC had similar accuracy as strain gauges, but also reported that DIC recorded very high strain gradients due to bone inhomogeneity. In Grassi et al. (2014) strain measurements were performed using a special set-up employing 2 high-speed cameras (1 Mpx, 3000 fps), creating stereovision and allowing for 3D-surface measurements of strain. There, femora were loaded in a single-leg-stance condition and the strains were measured on the anterior surface. To set a benchmark, strains, noise levels, and residual strains were reported at various stages of loading. Recently, Katz and Yosibash (2020) performed 3D-surface DIC measurements on the medial and lateral side of the femoral neck while loading the bones in a single-leg-stance. High strains were measured in the femoral neck around irregularities on the surface. As the bones were not loaded to failure it was not confirmed if these strains resulted in fracture.

## Digital volume correlation

Digital volume correlation (DVC) is based on the same concepts as DIC but rather than using 2D images obtained from digital cameras, 3D image volumes obtained from tomographic images are used. This enables measurements of internal strains and hence extends the surface approach of DIC to volumetric measurements.

The concept of using DVC on bone was first shown using a laboratory μCT (Bay et al., 1999). It was shown that displacements and strains could be effectively measured in a trabecular bone sample, before and after local failure. With laboratory μCT, strains in trabecular bone have been measured with an accuracy of ~0.1% with sub-volumes of ~200 μm (Palanca et al., 2015). With synchrotron CT a similar accuracy has been achieved with sub-volumes 10 times smaller (Tozzi et al., 2017). With these accuracies it has been possible to measure local strains in individual trabeculae reaching 6-7% while loading was still in the elastic region (Turunen et al., 2020).

The first study to perform DVC on bone at the organ scale was on a vertebra (Hussein et al., 2012). In another study on vertebrae injected with acrylic cement, the authors were able to show that damage initiated outside of the cemented region (Danesi et al., 2016). Martelli et al., (2021) created a complex loading device that allowed for loading of a full proximal femur simulating a single-leg-stance inside a laboratory μCT scanner. This way they were able to show that the subchondral bone was locally compressed 8-16% before fracture, and that fracture occurred in regions of peak tension and shear, adjacent to the location of peak compression.

DVC is a very promising technique but comes with three major limitations. First, the technique relies on the natural patterns and contrast within the sample, as it is not possible to apply a speckle pattern. Because of this, high-resolution and high-contrast images are required. Second, special loading devices are required that fit inside a 3D scanner. This means that most studies performing DVC on bone are studies where small bone samples are compressed in a laboratory μCT or at a synchrotron facility. Third, DVC is typically limited to less than 10 load steps and image sets. This is a result from high computational costs of running DVC due to its 3-dimensional nature, and the potential radiation damage caused by repeated imaging (Pena Fernandez et al., 2018).

## 3.5. Finite element models

As described in the previous section, intrinsic material properties can be determined from loading of small samples under simple loading conditions. Similarly, these material properties can be used to describe the mechanical behaviour of other similar samples with (sets of) partial differential equations. In biomechanics, problems often involve complex geometries, inhomogeneous material properties, and/or complex boundary conditions. The finite element (FE) method can be used to describe these problems numerically. In an FE model, the object is divided into a mesh consisting of multiple discrete elements with a simple shape. Each element can be assigned its own material property. By combining all element-specific equations and solving them, stress- and strain-fields can be calculated for complex geometries with local variations in material properties, and complex boundary conditions.

This method was first introduced in the field of orthopaedic biomechanics around 50 years ago (Brekelmans et al., 1972). With use of a 2D FE model of the femur, this study already showed the potential of FE models to investigate the influence of an altered geometry on the stress state. In the following decade, 3D FE models were introduced for various biomechanical problems. This included models of the femur and of a femur with a femoral component of a hip implant (Huiskes and Chao, 1983). Lotz et al. (1991) was the first to create FE models of the femur with varying material properties based on CT images. These models were able to accurately predict yield and fracture loads, when compared to *ex vivo* tests. However, they were not yet able to accurately predict surface stresses. Since then, models have been improved substantially, and multiple modelling strategies to create FE models of the proximal femur have been introduced (Johannesdottir et al., 2018).

The most common way to create FE models of the femur today is to use clinical CT images for segmentation of the femur geometry (Figure 3.5). The segmented femur is then subdivided into tetrahedral or hexahedral elements to create a mesh. Element sizes are often in the range of 1-3 mm, which results in a proximal femur with 20 000 – 200 000 elements. For each element, an apparent density ($\rho_{app}$) can be derived from the calibrated CT scans (Bonemat, Taddei et al., 2007). Using experimentally obtained modulus-density relationships, an initial Young's modulus ($E_0$) can be calculated and assigned to each element. For models of the proximal femur the most commonly used modulus-density relationships is:

$$E_0 = 6850\,\rho_{app}^{1.49} \qquad \text{(Morgan et al., 2003)}$$

At the surface of a model, the apparent density is often underestimated due to partial volume artifacts in the CT scans. These artifacts occur when two

materials with different densities fall within the same voxel, leading to an average grey value. To correct for these artifacts, elements at the surface of the mesh are sometimes assigned a minimum Young's modulus (Grassi et al., 2016; Helgason et al., 2008). Helgason et al. (2016) tested alternative methods for correction, but concluded that further investigation is required to find an optimal combination of partial volume artifact correction and modulus-density relationship. By assigning a separate modulus-density relationship for elements on the surface, strain predictions can be improved (Schileo et al., 2020).

FE models often include additional material parameters to account for, for example, non-linear, post-yield, and/or strain-rate dependent behaviour. Grassi et al. (2016) added strain-rate dependency by multiplying the Young's modulus of each element with an element-specific strain-rate correction factor every increment. This model also included strain-limits for yield and fracture. A good fracture-criterion is essential for accurately predicting the fracture strength. Initially, stress-based criteria for failure were most frequently implemented (Lotz et al., 1991; Keyak et al., 1997, 2005). However, later it was shown that strain-based criteria can sometimes better describe the failure of bone (Bayraktar et al., 2004; Schileo et al., 2008).

To ensure that FE models accurately describe the true mechanical behaviour of bone, they are validated against *ex vivo* mechanical tests (section 3.4). Fracture strength is the most relevant parameter for clinical use and therefore the parameter mostly used for validation (Johannesdottir et al., 2017; Viceconti et al., 2018). Multiple studies have shown similarly strong correlations between experimentally measured forces and fracture forces predicted by different FE models (Dall'Ara et al., 2013; Enns-Bray et al., 2018; Keyak et al., 2005; Koivumäki et al., 2012; Zysset et al., 2013). For further improvement of FE models and more accurate validation, surface strain measurements are often included in the experiments. Early studies used experiments with strain gauges for validation of FE models (Huiskes et al., 1983). More recent studies have started to validate the models against full-field DIC strain measurements (Gilchrist et al., 2013; Helgason et al., 2014; Grassi et al., 2016; Katz & Yosibash 2020). This method of validation has shown correlations between measured and predicted strains with an $R^2$ larger than 0.9 on the anterior side in a single-leg-stance loading condition (Grassi et al., 2016).

From measurements using strain gauges and DIC, discrepancies between experimentally measured and numerically predicted strains have been demonstrated (Grassi et al., 2012; Katz & Yosibash 2020). These discrepancies come largely from the highly irregular areas of the bone's surface on the superolateral side. With models based on µCT images, Bahaloo et al. (2018) was able to show that holes in the cortex (from vascularization) are likely involved in the initiation of fractures. It is therefore likely that inclusion of these

holes in macroscale models can improve the ability of FE models to accurately predict fracture events.

As mentioned, FE models can also be used to evaluate the mechanical properties of bone-implant or bone-cement constructs. Using such models, several orthopaedic implants have been evaluated as options for reinforcing the femoral neck to prevent fractures. Basafa et al. (2013, 2015) showed that FE models can predict the strength increase from augmentation of the femoral neck with PMMA. Additionally, they showed that FE models can be used to predict a patient-specific location for injection where a strong increase in fracture strength can be expected. Conversely, Varga et al. (2017) attempted to find a single general recommendation for prophylactic augmentation with PMMA. Based on the principles of Wolff's law an injection location was found that could lead to approximately 70% strength increase in osteoporotic patients. However, these results were not experimentally validated and it was not confirmed that the specific spreading of PMMA could be achieved clinically.

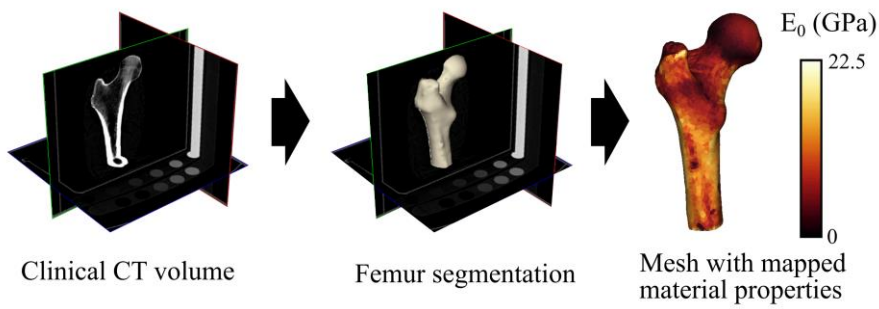


*Figure 3.5. A typical pipeline to create a finite element model from a calibrated clinical CT volume. From the CT volume the femur is segmented and meshed. The calibrated densities are used to assign a Young's modulus to each element.*

# 4. Material & Methods

In this chapter, the material and methods used in this thesis are outlined. First, the experiment in which femora were mechanically tested in a sideways fall loading condition is described (Study I). In the same section, the finite element (FE) models replicating these mechanical tests are described (Study II, III). Second, the studies conducted with a calcium sulphate/hydroxyapatite (CaS/HA) biomaterial are described (Study IV, V, VI). In each section, the subjects or specimens, and acquired images are introduced. This is followed by a description of the performed mechanical tests and/or FE analyses. Each section ends with an explanation of how the acquired data was analysed.

## 4.1. Sideways fall, mechanical testing and FE modelling (Study I, II, III)

Cadaveric femora were mechanically tested under a sideways fall loading condition and full-field strain measurements were performed through digital image correlation (DIC). FE models replicating the mechanical tests were validated against the mechanical tests and used to investigate the relationship between local strains and the resulting fracture.

### Subjects and imaging

Twelve proximal femora were collected from female donors without known conditions that affect bone metabolism (Ethical approval from The Finnish National Authority for Medicolegal Affairs: TEO, 5783/04/044/07). They were imaged with the modalities reported in Table 4.1 (Figure 4.1).

*Table 4.1. Modalities and details used for image aquisition in studies I, II, and III.*

| Imaging type | Instrument | Settings | Voxel size | Additional information |
|---|---|---|---|---|
| DXA | Lunar iDXA GE Healthcare | | 0.25 × 0.3 mm | |
| Clinical CT | Definition AS64 Siemens AG | 120 kVp 210 mAs | 0.4 × 0.4 × 0.6 mm | Calibrated with hydroxyapatite calibration phantom |
| µCT | Nikon XT H 255 | 100 kVp 0.2 mA | 52–60 µm (isotropic) | Full intact femora |
| µCT | MILabs U-CT | 65 kVp 0.13 mA | 60 µm (isotropic) | Parts of broken femora, after testing until failure |

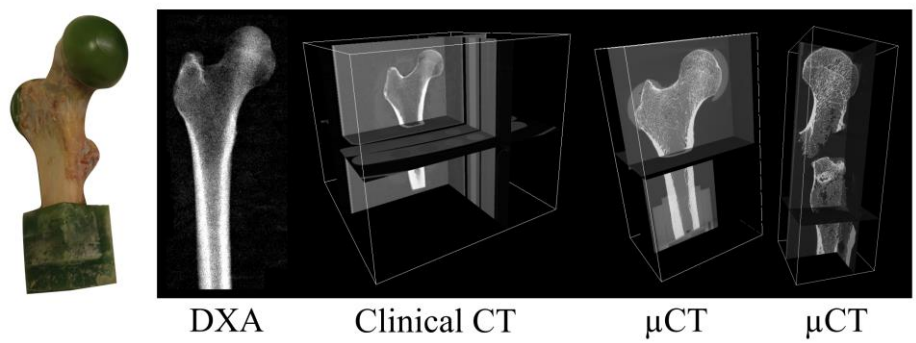


*Figure 4.1. Subjects and images acquired for studies I-III. From left to right: Photo of a proximal femur after embedding the femoral head, greater trochanter, and distal shaft in green epoxy; DXA scan of the femur to measure the aBMD in the femoral neck; Clinical CT scan to build FE models; µCT scan of the intact femur to build high-resolution FE models; µCT scan of the broken femur to accurately find the fracture surface.*

## Mechanical testing (study I)

The proximal femora were prepared for loading and digital image correlation (DIC) measurements. The soft tissue was removed and the distal end, femoral head, and greater trochanter were embedded in epoxy (Technovit® 4071, Kulzer GmbH). The superolateral and medial side were sprayed with matt white paint and black marker ink to create a black speckle pattern on a white background.

The loading setup was developed based on literature (Figure 4.2A) (Zani et al., 2015, 2013). The femur was placed in a configuration resembling a posterolateral fall, with an internal rotation of 15° and an adduction angle of 10° (Backman, 1957). The distal end was constrained to only allow rotation in the adduction/abduction directions. The greater trochanter rested over a system of two orthogonal linear bearings, and the load was applied to the femoral head (Instron® 8511.20, Instron Corp) at a controlled speed of 5 mm/s until macroscopic failure of the specimen was reached.

The experiments were recorded using two pairs of cameras recording the medial and superolateral sides of the femoral neck (Table 4.2). The recordings of the cameras were synchronized with the analogue recordings of the applied force (load cell M211-112, SensorData Technologies, Inc.).

*Table 4.2. Cameras and settings for recording images on the medial and superolateral side of the femoral neck to be used for DIC.*

| | **Medial cameras** | **Lateral cameras** |
|---|---|---|
| **Instrument** | Photron Fastcam Mini AX200 | Photron Fastcam-X 1280 PCI |
| **Recording speed** | 6400 fps | 500 fps |
| **Resolution** | 1024 × 1024 pixels<br>~20 pixel/mm | 1024 × 1280 pixels<br>~18 pixel/mm |
| **Pan angle** | ~16° | ~38° |

To obtain full-field strain measurements DIC was performed (Vic-3D v7, Correlated Solutions, Inc.). The correlation window size was chosen so that 1 standard deviation in the confidence interval of the matches between images ($\sigma$) would fall below 0.02 pixels. This resulted in a correlation window of 45 x 45 pixels for the medial cameras and 35 x 35 pixels for the lateral cameras. The node spacing was set to 9 pixels for the medial cameras and 5 pixels for the lateral cameras. The measured displacements were filtered using a low-pass filter in time at a cut-off frequency of 100 Hz. From the filtered displacement data, Green-Lagrange strain components were derived using a spatial decay filter of 5 data points.

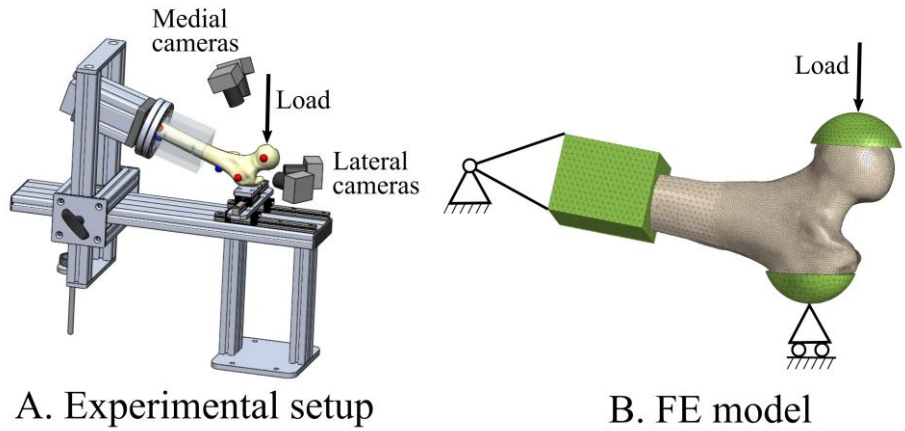


*Figure 4.2. A) Schematic of the mechanical testing setup for loading proximal femora in a sideways fall loading condition while recording the lateral and medial side with high-speed cameras. B) FE model of the proximal femur with epoxy. The loading conditions are set to replicate the mechanical tests.*

## FE analysis (study II, III)

As a basis for all FE models, bone elements were assigned an element specific tangent modulus. The apparent mineral density of each bone element was calculated based on the calibrated clinical CT scans using Bonemat (Taddei et al., 2007). From the apparent density, $\rho_{app}$, Young's moduli, $E_0$, were calculated based on the density-elasticity relationship:

$$E_0 = 6850 * \rho_{app}^{1.49} \qquad \text{(Morgan et al., 2003)}$$

The Poisson's ratio for bone was set to 0.4 (Reilly and Burstein, 1975). All epoxy elements were assigned a Young's modulus of 2500 MPa and a Poisson's ratio of 0.3. Nodes at the common surface of the epoxy and bone were shared, connecting the parts. All FE analyses were iteratively solved using the implicit FE solver Abaqus Standard (v2017 or v2019, Dassault Systèmes).

*Clinical CT based FE modelling (study II)*

The femur geometry was segmented from the clinical CT images by thresholding and applying manual corrections (Seg3D2, University of Utah). From the segmentation, a second-order tetrahedral mesh was created with element sizes of ~1 mm in and around the femoral neck, and ~3 mm for the rest (Hypermesh v17.0, Altair Engineering).

Each element was assigned an initial tangent modulus, $E_0$, as described previously. To overcome issues following from partial volume artifacts, a minimum $E_0$ of 2.5 GPa was assigned to all elements at the surface of the mesh. This material model included strain rate dependency, and different strain limit values for yield and failure under compression and tension (Grassi et al., 2016). The strain rate dependency and strain limits were based on the average principal strains for all elements within a 3 mm radius of the element. If the strain rate of an element exceeded the reference strain rate ($SR_{ref} > 0.5\%/\mathrm{s}$) (Bayraktar et al., 2004), $E_0$ was adjusted through multiplication with the strain rate correction factor:

$$SRCF = (SR_{elem}/SR_{ref})^{0.06}$$

where $SR_{elem}$ is the absolute maximum principal strain rate of the element. When element strain exceeded the yield strain limit (1.04% compression, 0.73% tension (Bayraktar et al., 2004)), the tangent modulus was reduced to 5.5% of its previous value (Reilly et al., 1974). A femur model was considered failed when the ultimate strain limit (2.11% in compression, 2.74% in tension (Reilly et al., 1974)) was exceeded for any of the elements on the surface of the femur. The force when the first element failed was taken as the predicted fracture force. The FE analyses were conducted by applying consecutive 0.05 mm increments with the time increment tuned to a 5 mm/s displacement rate.

*μCT based FE modelling (study III)*

High-resolution FE models including foramina on the superolateral side of the femoral neck were created. The femur was segmented from the μCT images of the intact femur (Seg3D2, University of Utah). The lateral side of the neck was selected as a region of interest (ROI) and semi-automatically segmented at the full resolution to include all surface irregularities. The rest of the femur was segmented from the μCT scans after downscaling four times. The segmentations were combined and a second-order tetrahedral mesh was created, where the elements had an edge length of ~0.2 mm in the ROI and ~3 mm in the rest of the femur (Figure 4.3).

The μCT based models used a different material model, while the boundary conditions were the same as for the clinical CT based models. Linear models were created with the initial tangent modulus based on the apparent density obtained from the μCT scans. The μCT scans were calibrated with the clinical CT scans by selecting a region in the air, marrow, and cortical bone in both scans, after which the grey values of the μCT images were adjusted using a linear fit. For these models a load of 10 newton was applied to each loaded node on the epoxy on the femoral head (5-9 nodes). The linear problem was then solved in one increment.

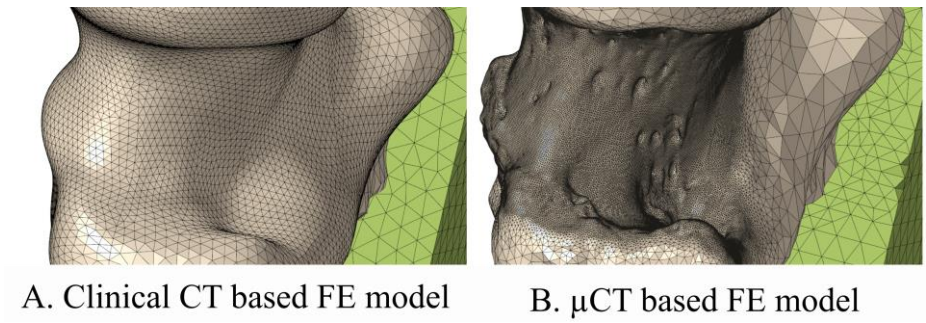


*Figure 4.3. Meshes of the lateral neck of an FE model based on A) clinical CT images and B) µCT images.*

## Data analysis

From the force–displacement data acquired during mechanical testing, peak force, and work-to-peak force were determined for each specimen. The strains measured with DIC were used to identify high strain regions before and at the peak force and at global failure.

The FE models based on clinical CT images were compared to the measured experimental outcomes of peak force, fracture onset, and surface strain:

- **Fracture force prediction**: The predicted and measured fracture forces were compared using linear regression analysis.
- **Fracture onset location**: The fracture onset locations predicted by the FE models were compared to the fracture line resulting from the experiment. The µCT scans of the broken bones were registered to the FE models (CloudCompare v2.8.1, www.cloudcompare.org/). The shortest distance between the predicted fracture initiation and the fracture line following from the mechanical loading was measured and reported.
- **Strain prediction**: Strain prediction accuracy was evaluated at a force corresponding to 90% of the experimentally measured peak force. The principal strains calculated by the FE analyses were compared to DIC measurements. The points from the DIC measurements were registered onto the surfaces of the FE models (CloudCompare v2.8.1, www.cloudcompare.org/). The size of the DIC point cloud was reduced before the comparison with the strains predicted by the FE models by removing the two outermost layers of points. Points where the confidence interval σ exceeded 0.02 pixels were excluded before correlation. A data comparison method was adopted, based on a

previous procedure (Grassi et al., 2013; 2016). For each element on the surface of the mesh, the smallest sphere circumscribing it was calculated. All DIC strain measurement points within the sphere were averaged and compared to the strain in the element. Linear regression analysis was performed to assess the correlation between the predicted and measured major and minor principal strains.

The strains predicted by the FE models based on μCT images were qualitatively compared to the fracture location and experimentally measured surface strain patterns.

## 4.2. Fracture strength after CaS/HA injection (study IV)

Strength increases resulting from an injection of CaS/HA were calculated with the use of FE models. FE models included variations in location, material properties, and volume of the injection.

### Subjects and imaging

Five femoral heads were collected from patients, diagnosed with osteoarthritis or osteonecrosis, that were about to receive a total hip replacement (THR) surgery. Before resection of the femoral head, the patients received an injection of 10 ml CaS/HA (Cerament™ Bone Void Filler, Bone Support AB) in their femoral neck (Ethical approval: Kaunas Regional Committee of Ethics of Biomedical Researches, BE-2-40). A needle with cannula was percutaneously introduced through the lateral cortex of the proximal femoral shaft at the same height as the upper part of the lesser trochanter. The cannula position in the femoral neck and material spreading during the injection was controlled and monitored with fluoroscopy (real time acquisition of X-ray projections). After material injection the THR surgery proceeded and the femoral head, injected with CaS/HA, was resected and collected. A total of 3 imaging modalities were used (Table 4.3; Figure 4.4). For the same study, images of five additional patients with fragility hip fractures were acquired (Ethical approval: Kaunas Regional Committee of Ethics of Biomedical Researches, BE-2-40).

*Table 4.3. Modalities and details used for image aquisition in study IV. All clinical CT scans were calibrated with a hydroxyapatite calibration phantom (QRM-BDC/6, Quality Assurance in Radiology and Medicine).*

*Five patients diagnosed with osteoarthritis or osteonecrosis undergoing THR*

| Imaging type | Instrument | Settings | Voxel size | Additional information |
|---|---|---|---|---|
| Clinical CT | Lightspeed Pro 16 GE Healthcare | 120 kVp 647-697 mA | 0.7-1 × 0.7-1 × 2.5 mm | Pelvic region Before surgery |
| Fluoroscopy | Arcadis Orbic mobile C-arm Siemens | 23 mA 2.3 kw | 0.6 mm focal spot | During injection of CaS/HA |
| Clinical CT | Lightspeed Pro 16 GE Healthcare | 120 kVp 198 mA | 0.5 × 0.5 × 2.5 mm | Femoral heads After resection |

*Five patients with fragility hip fractures*

| Imaging type | Instrument | Settings | Voxel size | Additional information |
|---|---|---|---|---|
| Clinical CT | Lightspeed Pro 16 GE Healthcare | 120 kVp 647-697 mA | 0.5-0.9 × 0.5-0.9 × 2.5 mm | Contralateral hip |
| DXA | Discovery Ci Hologic | | | Contralateral hip |

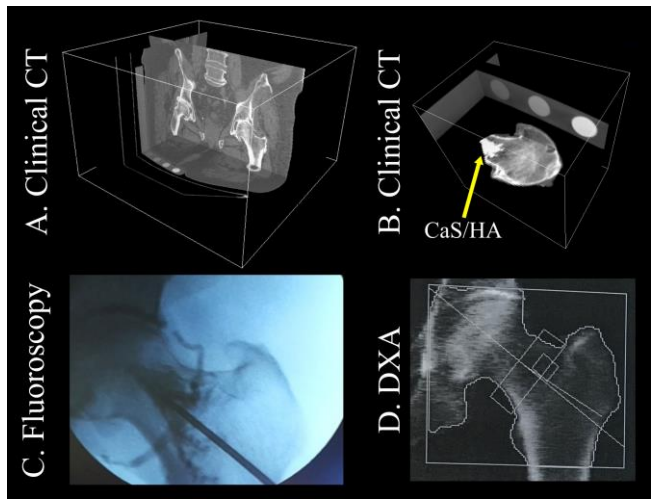


*Figure 4.4. Samples and images acquired for study IV. A) Clinical CT scans before surgery were used to create FE models of the proximal femur. B) Clinical CT scan of a femoral head after resection used to identify the region where CaS/HA spread. C) Fluoroscopy was used during CaS/HA injection to follow the spreading. D) DXA scans of the patients with fragility hip fractures to confirm that they were osteoporotic.*

## FE and data analysis

The FE models created in this study used the same basis as the FE models in study II and III (section 4.1).

The proximal femora were segmented from the clinical CT scans of all ten patients before surgery. The clinical CT images of the five resected femoral heads were used to segment the femoral head and the injected CaS/HA (Seg3D2, University of Utah). Since the injected CaS/HA volume was not fully located within the resected femoral heads, the segmentation of CaS/HA was extended with use of the fluoroscopy images to fill a total volume of 10 ml in the femoral neck. The segmentations of the proximal femur of the five patients undergoing THR and the respective femoral head, were aligned using an iterative closest point algorithm (CloudCompare v2.8.1, www.cloudcompare.org/). Second order tetrahedral elements were used to mesh the geometries of the proximal femur and the region with CaS/HA (total of ~100k elements and ~140k nodes (Hypermesh v17.0, Altair Engineering)). For the five hip fracture patients, who did not receive an injection, the geometry of the injected material from one of the THR patients was used. This geometry was manually aligned to fit in the femoral neck of the proximal femur geometries.

The region considered to contain CaS/HA was modelled as bone with the exception that the Young's modulus of each element was increased by 500 MPa. Additionally, the elements at the surface of the mesh were assigned a minimum Young's modulus of 500 MPa. Bone and CaS/HA were both regarded as isotropic linear elastic materials and all models were simulated in both single-leg-stance and sideways fall loading configurations (Figure 3.3). A strain-based failure criterion was implemented to calculate the fracture strength (Schileo et al., 2014). For each of the nodes on the surface the average principal strains in a 3mm radius are calculated. The strains and applied load are increased until a major principal strain of 0.73% or minor principal strain of -1.04% is reached for one of the nodes (Bayraktar et al., 2004). The node that first fails is the fracture location and the load required to reach this strain is the fracture strength. The fracture strength was calculated for each femur, with and without the increased modulus in the elements representing CaS/HA. Through comparison of the fracture strength calculated by the two respective models, the relative increase in fracture strength was determined for each simulated injection.

In addition to the models with the baseline injection, three modes of variation in injection were analysed: change in location in the femoral neck (7 additional locations (Figure 4.5)), change in the modulus of the injected material (1000 MPa and 2000 MPa), and change in injected volume (Figure 4.5). In all models, the mesh remained unchanged, and elements at the surface of the mesh were not allowed to be part of the injected region.

For the variations in injected location and stiffness, the relative strength increase with respect to the femur without injection was determined. For the variation in injected volume, the relative strength increase with respect to the baseline injection was determined to assess the additional strength increase from the further increase in injected volume.

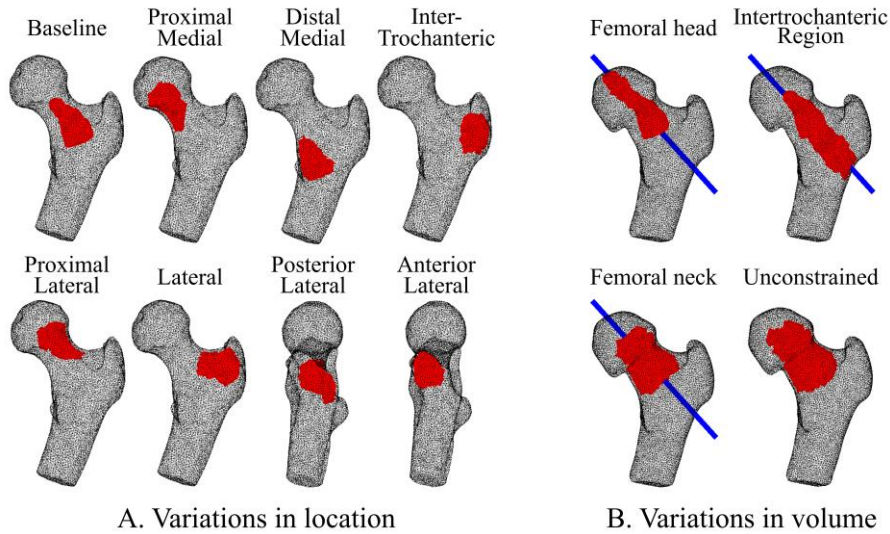


*Figure 4.5. A) The baseline and seven variations in location of 10 ml of injected material. B) The modelled directions for the volume increase of the injection. The directions for volume increase were limited to: the femoral head along the direction of the injection; the intertrochanteric region along the direction of the injection; the femoral neck perpendicular to the direction of the injection; all directions.*

## 4.3. Screw pullout strength with CaS/HA (study V)

The increase in immediate fixation that CaS/HA can offer dynamic hip screws (DHS) was evaluated through pullout tests conducted on synthetic and human bone.

### Specimens and imaging

To perform the mechanical tests, the following material was used (Figure 4.6):

- Synthetic foam blocks with structural and mechanical properties similar to that of trabecular bone (Sawbones Europe):
    - **Low-density:** 15% bone volume fraction (mimicking osteoporotic bone)
    - **High-density:** 31% bone volume fraction (mimicking healthy bone)

- Human femoral heads (n=29) harvested and banked from patients undergoing partial or total hip replacement after a low-energy femoral neck fracture. The heads were surgically removed using an extractor screw or hook, leaving a clearly visible hole in the trabecular bone. The patients gave their informed consent to the retention and use of their tissue in accordance with Kaunas hospital guidelines and the relevant EU legislation.
- Dynamic hip screws (115 mm, Auxein Medical, Haryana, India):
    - **Cannulated:** Screws with a single central cannula. Material injected through these screws is purely deposited at the tip of the screws.
    - **Fenestrated:** Screws with a single central cannula and 6 fenestrations (holes with a 1.5 mm diameter) in the threads of the screw. Material injected through these screws is deposited at the tip of the screws and directly in the threads through the fenestrations.

The collected femoral heads were imaged before and after insertion of the screws and injection of CaS/HA (Table 4.4).

*Table 4.4. Modalities and details used for image aquisition in study V.*

| Imaging type | Instrument | Settings | Voxel size | Additional information |
|---|---|---|---|---|
| µCT | MILabs U-CT | 65 kVp<br>0.13 mA | 40 µm<br>(isotropic) | Hydroxyapatite phantoms included (250 and 750 mg/cm$^3$) |
| Clinical radiography | Discovery XR656<br>GE Healthcare | | | After insertion of the screws and injection of CaS/HA |

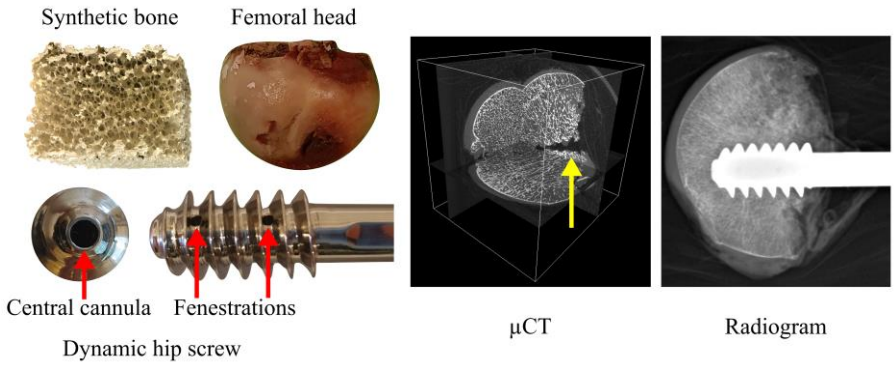


*Figure 4.6. Samples and images acquired for study V. From left to right: Synthetic bone block; femoral head; Dynamic hip screws (cannulated and fenestrated); µCT scan of a femoral head (the arrow indicates the hole left by the extractor screw); Radiographic image of a femoral head after screw insertion.*

## Mechanical testing

*Synthetic bone preparation*

The synthetic bone was cut into blocks with a size of 6 x 5.5 x 4 cm using a hand saw. A 3 cm deep hole with 6 mm diameter was predrilled in the centre of each block. The blocks were divided into three groups:

- **Empty**: Cannulated screws were inserted 3 cm.
- **Cannulated**: Cannulated screws were inserted 2 cm, after which 2 ml CaS/HA was injected and the screw was inserted an additional 1 cm.
- **Fenestrated**: Fenestrated screws were inserted 3 cm, after which 2 ml CaS/HA was injected

*Human femoral head preparation*

The position for insertion of the DHS was planned for each femoral head from the µCT images based on segmentation of the femoral head and the hole left by the extractor screw (Seg3D2, University of Utah). The fracture surface of the femoral heads was cut flat using a diamond band saw (Exact Technologies Inc).

Due to the smaller size of the femoral heads compared to the synthetic bone, the insertion depth was reduced. In the femoral heads, a 20 mm deep hole with 8 mm diameter was predrilled and the same three groups, as used for the synthetic bone, were created:

- **Empty**: Cannulated screws were inserted 2 cm.
- **Cannulated**: Cannulated screws were inserted 1 cm, after which 2 ml CaS/HA was injected and the screw was inserted an additional 1 cm.
- **Fenestrated**: Fenestrated screws were inserted 2 cm, after which 2 ml CaS/HA was injected

*Pullout test*

Pullout tests were performed using a custom pullout setup (Figure 4.7). A metal box with two open sides and a hole in the top was clamped to the bottom of the loading device (Instron® 8511.20, Instron Corp). The DHS with the bone attached was passed through the hole and connected to the top of the loading device. The screw was then loaded at a displacement rate of 0.5 mm/s until failure.

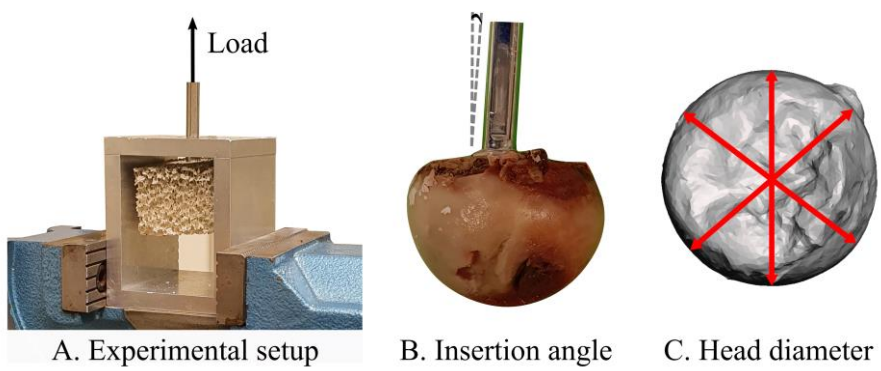


*Figure 4.7. A) Photo of the custom pullout setup with a synthetic bone block. B) Representation of how the insertion angle of the screw is measured. C) Schematic of how the femoral head diameter is measured based on a segmentation of the head from the µCT images. The head diameter was defined as the average of three measured diameters.*

### Data analysis

The force-displacement curves from all pullout tests were analysed by measuring the peak force, the stiffness in the linear region, and the work to peak force. Statistical comparisons between the groups were made using a Kruskal-Wallis test and a Dunn's post-hoc test for multiple comparison.

For the femoral heads additional parameters were measured:

- **Bone volume/total volume (BV/TV):** In the µCT images, the region at the location of screw insertion was selected and segmented using a threshold of 450 mg/cm$^3$. In case the DHS insertion site covered the hole left from the extraction, this hole was excluded from the BV/TV measurement.
- **Insertion angle:** From two photos of the femoral head with the screw after insertion, the insertion angle was determined as the angle between the DHS and the normal to the flat surface after cutting the femoral heads (Figure 4.7).
- **Head diameter:** The head diameter was measured from segmentations of the femoral head (Figure 4.7).

The effect of these additional parameters on the mechanical outcome of the pullout was investigated per group using linear regression analysis.

## 4.4. Bone-CaS/HA mechanical behaviour (study VI)

To investigate the mechanical behaviour of the composite of bone and CaS/HA, *in situ* compression tests were performed during imaging using synchrotron CT. Tests were performed on specimens of trabecular bone, CaS/HA, and the composite of the two.

### Specimens, imaging, and mechanical testing

Two femoral heads collected from the patients undergoing THR (study IV) were used for the collection of eleven cylindrical trabecular bone specimens (diameter: 6 mm, height: 7.5 mm) (Figure 4.8). The bone marrow was removed from all plugs. In 5 plugs, CaS/HA (Bone Void Filler, BoneSupport AB) was inserted. One cylindrical sample of pure CaS/HA was created.

The plugs were mechanically loaded *in situ* and imaged with synchrotron CT (X02DA TOMCAT beamline, Swiss Light Source, Paul Scherrer Institute, Switzerland). The specimens were compressed at a displacement rate of 0.3 mm/min using a custom-made loading device (Turunen et al., 2020). Tomograms were taken before loading and at increments of 0.15 mm (~2% strain) until failure of the specimens. The projections were corrected using flat-field and dark-field images, reconstructed in phase-mode. The resulting image volumes had an isotropic voxel size of 2.75 µm and a field of view of 11 x 11 x 3 $mm^3$. As the specimens were taller than the field of view (7.5 mm against 3 mm), specimens were moved vertically and scanned three to four times sequentially to cover the full height. The multiple image stacks acquired were stitched after reconstruction.

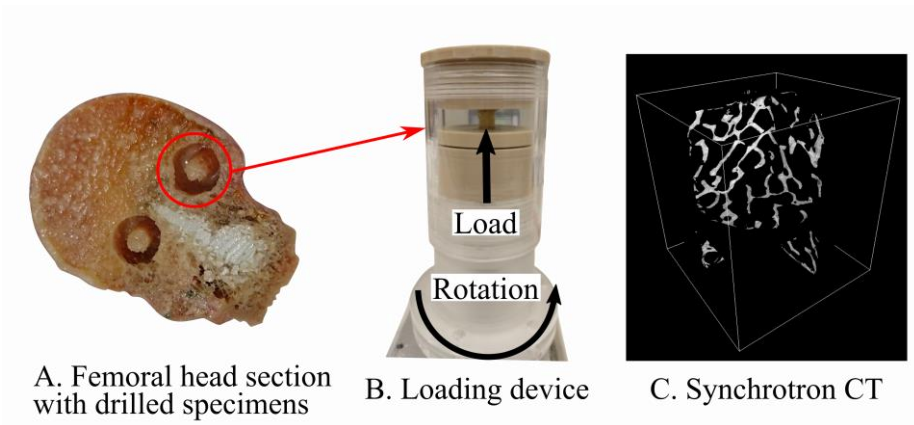


*Figure 4.8. Samples and images acquired for study VI. A) Half a femoral head, where 2 plugs have been drilled. B) The custom-made loading device for in situ loading. C) A synchrotron CT volume of a full bone specimen after stitching the stacks.*

## Data analysis

From the force-displacement curves, stress and strain were calculated. Change in height of the specimen was measured from the image stacks to correct the strain for compliance in the loading device. From the stress-strain curves, ultimate stress, ultimate strain, apparent modulus, and toughness were determined.

BV/TV was calculated for all specimens from the images acquired before injection of the CaS/HA. The CaS/HA volume/total volume (CV/TV) was determined from the images of the unloaded composite and CaS/HA specimens.

One specimen from each group was selected for analysis through digital volume correlation (DVC). DVC was used to visualize the displacements in the whole specimen, from which regions where damage appeared could be identified. Before running DVC, a 3D median filter of ±1 voxel was applied on the images and the background was removed through thresholding.

DVC was run using the open-source software TomoWarp2 (Tudisco et al. 2017). First, DVC was run on the entire sample volumes after downscaling four times. A correlation window of ±7 voxels and a node spacing of 7 voxels were used. Second, DVC was run on longitudinal cross-sections (~7.5 x 6 x 0.3 mm) kept at full resolution. A correlation window of ±10 voxels and a node spacing of 10 voxels were used. Before each load step, the displacements were filtered using an outlier filter followed by a ±1 voxel median filter. At each load step, the filtered displacements were used to calculate the maximum shear strains. The strain maps at the fourth load step (~8% global strain) were used to identify regions where damage occurred. The progression of damage in these regions was then visually inspected throughout all load steps.

# 5. Results

In this chapter, the main results and findings from the studies described in the previous chapter are presented. Each section starts with a short summary of the methods, followed by a summary of the results of each study.

## Sideways fall mechanical testing (study I)

Cadaveric femora were mechanically tested under a sideways fall loading condition and full-field strain measurements were performed and analysed with digital image correlation (DIC).

Peak force of the samples varied from 1515 N, for an 85-year-old with a femoral neck aBMD of 0.43 g/cm$^2$, to 5477 N, for a 22-year-old with a femoral neck aBMD of 0.97 g/cm$^2$ (Table 5.1). With exception of one subject, initial damage was observed under compression in the lateral neck. After the peak force was reached, the severity of the damage on the lateral side gradually increased. On the medial side of the neck, no damage was observed until complete failure occurred under tension.

From the DIC analysis, it was observed that the compressive strains on the lateral side gradually increased until the peak force was reached (Figure 5.1). After reaching the peak force, the deformation became too large for accurate strain measurements. Whereas, on the medial side, strains did not increase substantially until after the peak force was reached.

*Table 5.1. Subject age at time of death, bone mineral density of the femoral neck, peak force, and work to peak force for all subjects. The subjects marked are the weakest (red) and the strongest (green) subjects, and the subject shown in figures 5.1 and 5.2 (yellow).*

| ID | Age [yrs.] | aBMD [g/cm$^2$] | Peak force [N] | Work to peak force [Nmm] |
|---|---|---|---|---|
| CAD045 | 70 | 0.82 | 3975 | 8358 |
| CAD046 | 83 | 0.67 | 2383 | 3728 |
| CAD047 | 68 | 0.99 | 4451 | 8876 |
| CAD049 | 85 | 0.43 | 1515 | 1705 |
| CAD050 | 22 | 0.97 | 5477 | 23250 |
| CAD051 | 67 | 1.05 | 4531 | 8895 |
| CAD052 | 68 | 0.64 | 4246 | 12642 |
| CAD053 | 88 | 0.74 | 4706 | 12938 |
| CAD054 | 81 | 0.55 | 2520 | 3443 |
| CAD055 | 80 | 0.74 | 3523 | 6259 |
| CAD057 | 71 | 0.83 | 4718 | 7437 |
| CAD060 | 59 | 0.92 | 5325 | 16901 |

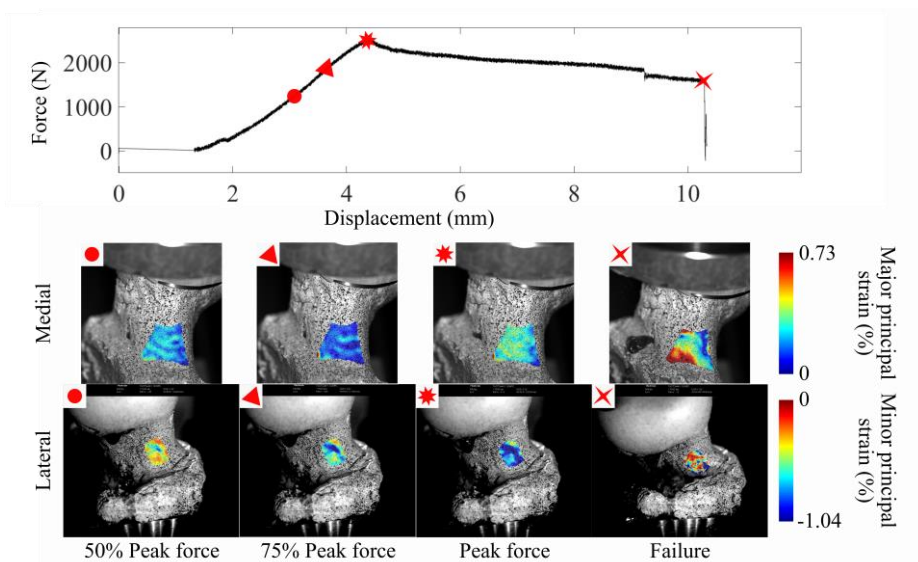


*Figure 5.1. Force-displacement curve of one subject and the strains calculated with DIC at points on the load curve. The strain initially increased most on the lateral side under compression. After reaching the peak force the tensile strain on the medial side started increasing.*

## Sideways fall FE modelling (study II, III)

Two sets of FE models were created and compared to each other and to the experimental outcome of study I. First, FE models based on clinical CT images were used for validation of an established modelling procedure (Grassi et al., 2016). Second, FE models based on µCT images were used to investigate the influence of local strains on the resulting fracture.

*Fracture force & location*

The FE models based on clinical CT images predicted the fracture forces with high accuracy ($R^2 = 0.92$). The predicted fracture location was, for all models, under compression on the lateral side of the neck. Eight out of the twelve predicted fracture locations were within 3 mm of the experimental fracture line. The other four predictions were all proximal to the experimental fracture on the lateral neck.

*Strains*

The FE models based on clinical CT images predicted the strains on the medial side with high accuracy ($R^2$ range: 0.82–0.96) (Figure 5.2). On the lateral side the accuracy of the strain prediction varied more between subjects ($R^2$ range: 0.67–0.98).

The µCT images of the intact femur were compared to the DIC measurements and FE models. In regions where experimentally measured strains were higher than the FE predicted strains, the bone surface was more irregular, often in the form of a hole in the cortex.

*µCT based FE models*

The linear FE models predicted high strains where often the highest strains were present inside foramina (Figure 5.3). This is in agreement with the experimentally measured strains. However, the high predicted strains were limited to small regions. The experimentally observed fracture path did not necessarily go through the foramina where the highest strains were predicted. Regions where the highest strains were predicted after excluding foramina corresponded better with the experimental fracture path.

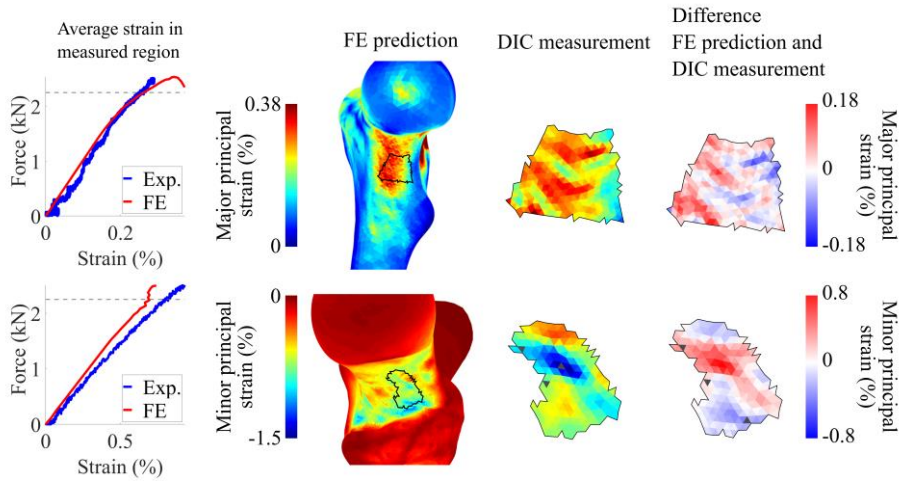


*Figure 5.2. A comparison between FE predicted and experimentally measured strains on the medial (top) and lateral (bottom) side of the femoral neck. The force strain curves show the average measured and predicted strains in the region where strains were measured using DIC. The dotted grey line indicates the force at which the measured and predicted strains are compared. On the lateral side high strains were measured around a foramen that were not predicted by the FE model.*

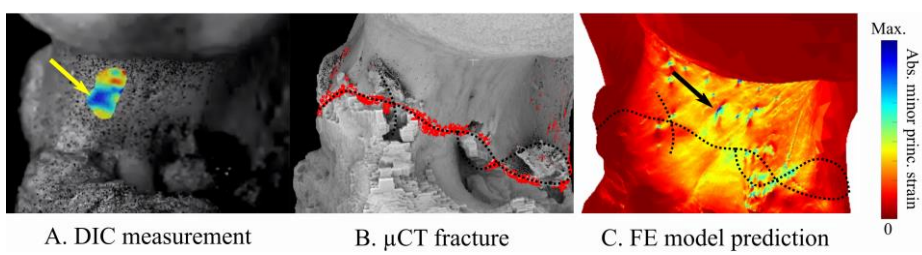


*Figure 5.3. A) Strains measured using DIC. B) Registered µCT segmentations showing the fractured region. C) Strains predicted by the linear FE model based on the µCT images. The black dotted lines represent the experimentally fractured region. The arrows point at the high strains measured and predicted in and around the same foramen.*

## Fracture strength after CaS/HA injection (study IV)

Patients undergoing THR received an injection of CaS/HA into the femoral neck before resection of the femoral head. Baseline FE models of the proximal femur with the injection were created. Additionally, variations in injection location, stiffness, and volume of CaS/HA were modelled. The increase in fracture strength following the injections of CaS/HA were calculated and compared.

From the baseline injection, the FE models predicted a maximum increase in fracture strength of 7% in single-leg-stance and 9% in sideways fall, for the patients with fragility hip fractures (Figure 5.4). For the patients without osteoporosis, the maximum calculated strength increase was 3% in single-leg-stance and 5% in sideways fall.

Altering the location of the injection proved to have the largest effect on the fracture strength. A maximum increase of 26% under sideways fall loading was calculated when the injected volume was placed on the lateral side of the neck. For some injection locations, the calculated fracture strength decreased. This effect was most prominent with the injection in a more proximal lateral position. An injection placed in a medial position resulted in very little change in fracture strength.

Further increasing the stiffness of the assumed biomaterial (1000 MPa, and 2000 MPa) also further increased the calculated fracture strength. However, the highest relative increase followed from the initial 500 MPa in material stiffness.

Increasing the volume of the injection also increased the calculated fracture strength. The largest effect per unit of injected volume was observed when the volume was increased toward the greater trochanter. The highest total increase in fracture strength was calculated for an increase in volume in all directions.

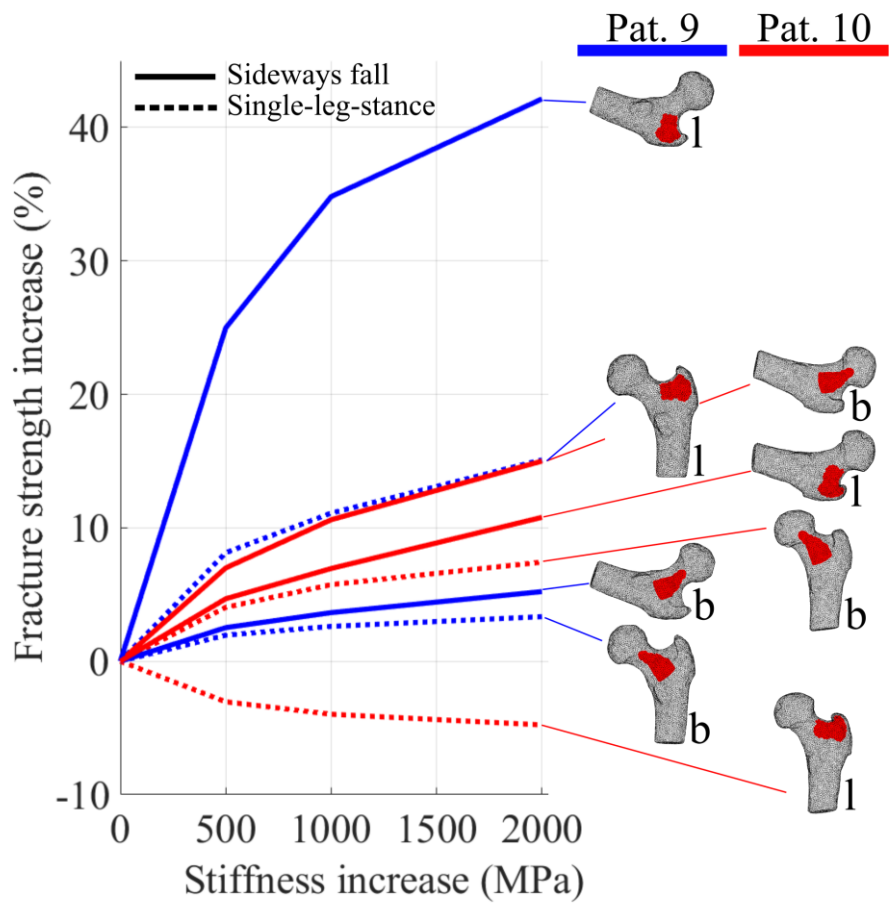


*Figure 5.4. The fracture strength increase compared to no injection for the two patients (9 and 10) with the lowest aBMD. The increase in fracture strength is shown as a function of the stiffness of the biomaterial for the baseline (b) injection and lateral (l) injection location, for both loading conditions.*

## Screw pullout strength with CaS/HA (study V)

Dynamic hip screws were inserted in blocks of synthetic bone and human bones, with and without injection of CaS/HA. Pullout tests were conducted to compare the stability of the screws.

*Mechanical testing*

In the synthetic bone blocks, the highest pullout forces were recorded with the fenestrated screws after CaS/HA injection (Figure 5.5). For the low-density blocks, the pullout forces recorded for the cannulated group were higher than in the empty group. In the high-density blocks, there were no significant differences between the cannulated and empty groups. In the human femoral heads, there were no differences in mechanical behaviour between any of the groups.

*Image analysis*

After pullout of the screws from the synthetic bone, the amount of CaS/HA left on the screw varied between groups (Figure 5.6). From the radiographic images of the femoral heads, it was observed that CaS/HA was mostly deposited at the tip of the screw after injection through the cannulated screws. With the fenestrated screws there was no clear spreading of CaS/HA in the bone. Instead, CaS/HA was deposited at the cut surface of the bone.

Linear regression analysis for parameters measured before testing (i.e., BV/TV, insertion angle, and head diameter) and mechanical parameters, showed several correlations: In the empty group, a higher BV/TV led to a higher pullout strength ($R^2 = 0.58$, $p = 0.006$) and higher work to peak force ($R^2 = 0.39$, $p = 0.04$). In the cannulated group, the insertion angle correlated with the stiffness ($R^2 = 0.70$, $p = 0.02$). In the fenestrated group, no significant correlations between parameters were found.

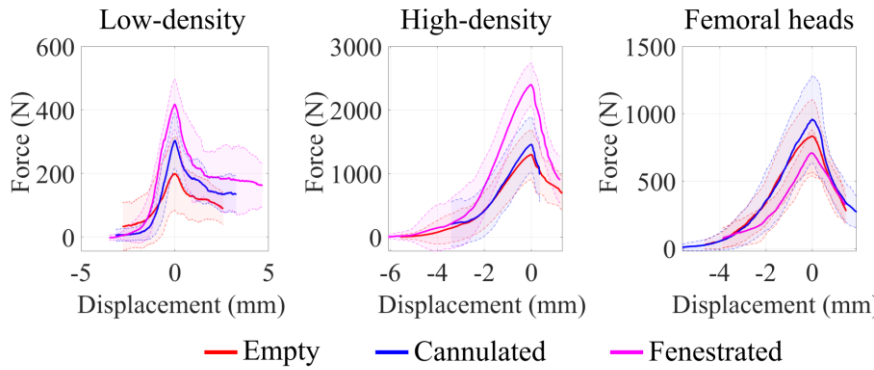


*Figure 5.5. Force-displacement curves for the synthetic low- and high-density bone and the human femoral heads, shown as mean (solid lines) and standard deviations (shaded area). To obtain a representative measure for the mean and standard deviation of the curves the displacement to peak force was first subtracted from each individual curve to centre the peak at 0 mm displacement.*

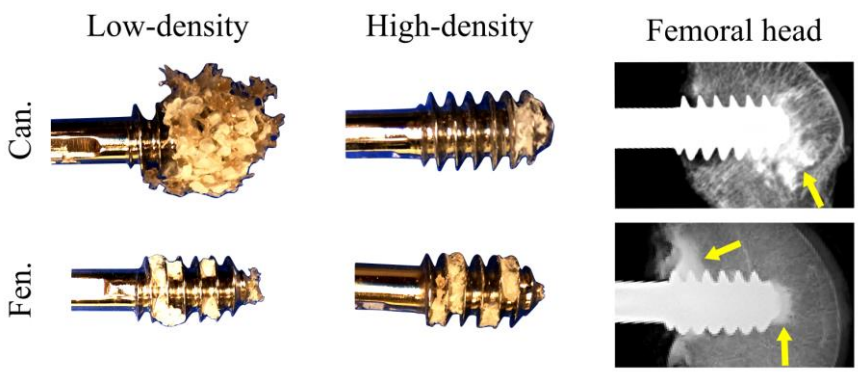


*Figure 5.6. Left) Photos after pullout from the synthetic bone showing the remaining material on the cannulated and fenestrated screws after pullout. Radiographic images from the screws inserted in the human femoral heads. The arrows indicate where the CaS/HA has spread.*

## Bone-CaS/HA mechanical behaviour (study VI)

Cylindrical specimens of bone, CaS/HA, and the composite of the two were compressed *in situ* during imaging with synchrotron CT. The mechanical behaviour, and damage initiation and propagation were compared qualitatively between specimen types.

*Mechanical testing*

There were clear differences in the mechanical behaviour between the three groups (Figure 5.7). The bone specimens reached ultimate stresses of 2.1-5.8 MPa, while the CaS/HA specimen reached 16.9 MPa. The ultimate stresses of the composite samples reached intermediary values (8.3-11.0 MPa). CaS/HA was observed to be more brittle than the composite and bone samples, with a strain at ultimate stress of 0.006 compared to 0.037-0.056 for the bone, and 0.019-0.064 for the composite specimens. Additionally, a longer post-yield region of the composite specimens also led to higher toughness than pure CaS/HA (0.33-0.60 J/mm$^3$ vs 0.28 J/mm$^3$).

*Image analysis*

DVC analysis was used to identify regions where failure occurred during loading. In these regions, the damage initiation and propagation was observed for the first four load steps (Figure 5.8).

In the bone specimen, regions of high local strain revealed locations where the bone started bending, buckling, and cracking. This damage propagated gradually throughout the loading.

In the CaS/HA specimen, global failure was observed with large cracks propagating through the sample. There was no clear deformation or increase in strain before cracks opened in the second load step.

In the composite specimen, three different modes of damage were observed. First, microcracks in the CaS/HA were observed throughout the sample. Second, the bone and the CaS/HA was found to separate from each other in multiple locations. Third, compaction of the CaS/HA was observed as an increase in brightness (not visible in the region of interest displayed in Figure 5.8).

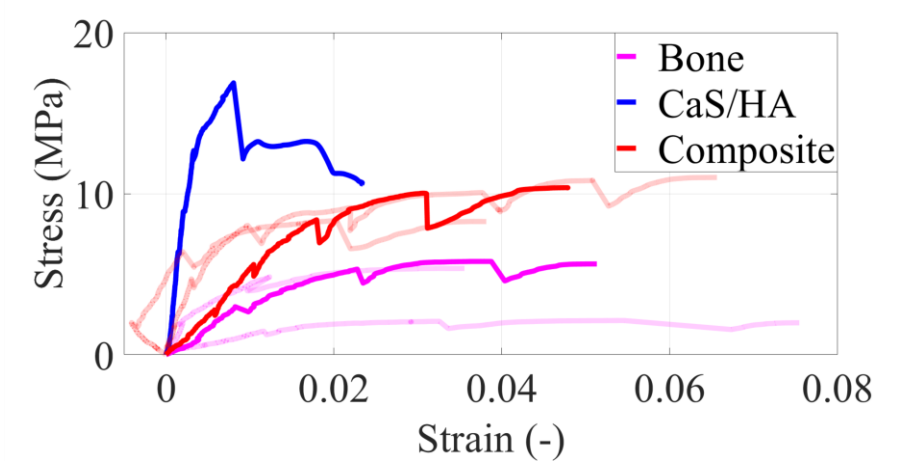


*Figure 5.7. Force-displacement curves of all specimens. The opaque lines indicate the specimens used for DVC analysis and inspection of detailed damage progression.*

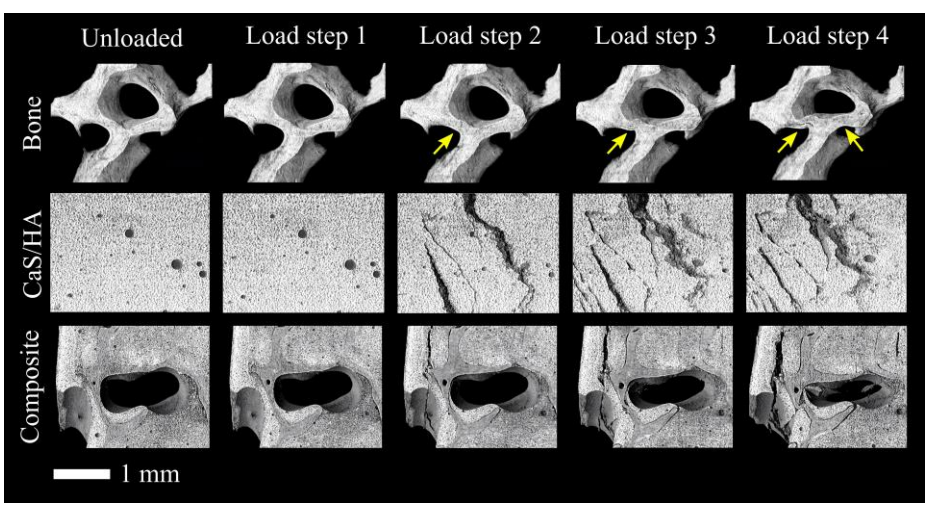


*Figure 5.8. Progression of damage through the first four load steps in regions where clear damage occurred. The arrows indicate where bending and cracking can be observed in the bone specimen.*

# 6. Discussion

The overall aim of the work in this thesis was to investigate ways that could improve current hip fracture strength prediction tools, and fracture prevention and repair methods. In study I, femora were mechanically loaded in a fall loading condition until failure while measuring strains on the medial and lateral side of the femoral neck. This experiment was used to validate a finite element (FE) modelling approach (study II). For these studies, μCT images were taken before and after the experiment. The images were used to create models with a higher resolution to investigate the strains and damage developing from surface irregularities on the superolateral femoral neck (study III). Similar models were used in study IV to investigate how the strength of the proximal femur can be increased through injection of calcium sulphate/hydroxyapatite (CaS/HA). Following this, screw pullout experiments were conducted to determine if CaS/HA can also improve the stability of dynamic hip screws, used to aid in the repair of hip fractures (study V). Finally, to further improve our understanding of the mechanical behaviour of CaS/HA in combination with bone, experiments were conducted where small cylindrical specimens of bone and CaS/HA were loaded during imaging with synchrotron CT (study VI).

## 6.1. General

**Sideways fall mechanical testing**

The mechanical testing of the femora under sideways fall was set up with the aim to gain insight in the mechanical behaviour of the femur during a fall. The loading setup was developed so the adduction and internal rotation angles of the proximal femora could easily be set to a 10° adduction angle and a 15° internal rotation angle. These angles are considered to be clinically relevant, since posterolateral falls are most associated with a high hip fracture incidence (Greenspan et al., 1998). This specific loading condition is commonly used for experimental mechanical tests and for FE analyses, allowing for detailed comparison of the results with other similar studies (Heini et al., 2004; De

Bakker et al., 2009; Koivumäki et al., 2012; Dall'Ara et al., 2013; Zani et al., 2015).

The mechanical testing showed that hip fractures initiate under compression in the superolateral neck. This finding is supported by similar experimental studies (De Bakker et al., 2009; Zani et al., 2015). A study with a more complex experimental setup, including a pelvis and soft tissue, also reported similar fracture events (Fleps et al., 2019). Even in a clinical setting, compression-induced failure has been observed for hip fractures (Tang et al. 2017). This further supports the notion that the presented experimental setup can be used to investigate clinically relevant fracture behaviour.

The analysis with digital image correlation (DIC) showed that the strains could be accurately measured over a full surface on the femur. Interestingly, in many cases local strains exceeded yield limits determined for trabecular bone (1.04%, Bayraktar et al., 2004) before the peak force was reached. Through comparison with µCT images of the femur, it was revealed that the underlying factor contributing to these strains was generally high surface irregularity in the form of a hole in the cortex. One can speculate that this means that high strains around these holes do not necessarily lead to immediate global failure. It could also be argued that the high strains were measured as a result from pressure building up behind the applied layer of paint, as leakage of bone marrow was observed through several holes. However, the high strains were often more distributed than directly on top of the hole, suggesting that the strains at least partially represent the strain of the bone itself. A study by Katz and Yosibash (2020) supports this idea. In their study, femora were loaded in a stance loading condition and DIC analysis was performed on the lateral neck. For this loading position, relatively high tensile strains were recorded around the holes in the neck.

The first study nicely illustrates the relevance strength predictions can have for clinical risk assessment. Two of the femora had similar aBMD measurements (0.64 g/cm$^2$ (CAD052) and 0.67 g/cm$^2$ (CAD046)), while the measured peak force of the one with the slightly lower aBMD measurement (4246 N (CAD052)) was nearly double that of the other (2383 N (CAD046)). Based on aBMD alone, these two subjects would likely have been classified with the same risk of fracture, even though looking at the strength of the femora they should be classified differently.

## FE modelling

In studies II, III, and IV, FE analyses were performed on proximal femora, all with slightly different approaches and purposes.

In study II, FE analyses were performed using a modelling approach already validated for a single-leg-stance loading condition (Grassi et al., 2016). The previous validation was performed on only three subjects, which was regarded as the major limitation. In this thesis work, twelve subjects were tested and the validation was performed in a more clinically relevant loading condition. The fracture strength predicted by these models correlated well with the experimentally measured peak forces ($R^2$ = 0.92). The predictive strength of these models was similar to, if not slightly better than, those presented in studies proposing other modelling approaches for the same loading conditions ($R^2$ = 0.87, (Koivumäki et al., 2012); $R^2$ = 0.85, (Dall'Ara et al., 2013)).

From the included comparison between predicted principal strains against the strains measured with DIC, it was possible to determine with more precision how accurate the FE models describe the actual mechanical behaviour of the femur. Especially the comparison to the strain measurements on the lateral side of the femoral neck is of great interest, as this has repeatedly been shown as the region where fracture initiates (De Bakker et al., 2009; Zani et al., 2015). Strain gauges have long been the gold standard for quantitative strain validation of FE models. Since strain gauges require a clean flat surface, measurements on the superolateral neck were often avoided. However, Grassi et al. (2012) presented strain measurements with one strain gauge in the femoral neck, where the validation of FE models against the minimum principal strain measurements resulted in overpredictions of 30%. The origin of this discrepancy was speculated to come from anisotropy, but this could not be confirmed. The comparison between predicted and measured strains presented in study II showed strong correlations. However, it was also seen that the locally high measured strains resulting from underlying surface irregularities were not accurately predicted by the FE models. This suggests that inclusion of these surface irregularities could improve the ability of the models to accurately predict the strains, potentially more so than inclusion of anisotropy could.

The versatility of the modelling approach was shown by validating it for two separate loading conditions. The proposed modelling approach was able to overcome several limitations posed in other approaches. Some FE modelling approaches may require a calibration set, reducing the number of models that can be used for validation (Keyak et al., 2005). Another approach would require calibration of the apparent density values with the use of µCT images (Zysset et al., 2013). In contrast, the present approach uses parameters obtained from previous independent studies and requires no internal calibration of input parameters, making it readily available to be used with a calibrated clinical CT scan as the only requirement.

In the experimental measurements, high strains were measured that in several cases could not be predicted by the FE models based on clinical CT scans. In

study III, models were created based on µCT images. With the higher resolution of the µCT images, it was possible to create models including foramina and other surface irregularities. These models showed that the high strains measured by DIC can indeed originate from the foramina.

In study IV, FE models were used to investigate the effect that an injection of CaS/HA has on the predicted fracture strength. Compared to the models used in study II and III, a simpler linear elastic material model was used, with a previously validated fracture criterion (Schileo et al., 2014). Due to the simplicity of this model, it was possible to run the hundreds of various models within a reasonable time. Additionally, for this comparative study predicting the exact fracture strength was not of primary importance.

The baseline injection location showed a limited increase in fracture strength. However, this injection was purposely placed centrally in the femoral neck to investigate the ability of CaS/HA to spread in the trabecular structure. The other investigated locations for CaS/HA injection were selected to be closer to the cortical bone, but still clinically applicable. These locations showed higher increases in fracture strength. When optimizing the locations for a maximum increase in fracture strength even higher increase in strength can be expected (Varga et al., 2017). However, in this case it is likely that the clinical applicability is lost. With special tools for injection, it could be possible to find a good cut-off between optimal fracture strength increase and clinical applicability (Basafa et al., 2015).

The mechanical properties of CaS/HA were represented in this study by applying an increase in Young's modulus of the present bone. The modulus was approximated from data received from the manufacturer of the material. This data only presented values on the pure material and not about the composite behaviour after injection in bone. We therefore also decided to vary this increase in modulus to get a better feeling for the effect of the stiffness in combination with the presented variations in location. Regardless of the exact modulus of the combination of bone and CaS/HA, the material properties will likely change greatly within the first weeks-months after injection as the CaS phase is resorbed (Wang et al., 2016). One of the advantages of CaS/HA is that it can function as a delivery system or recruitment platform for bone active drugs (Raina et al., 2016, 2019). Inclusion of drugs increases the bone density (Sirka et al., 2018), which would lead to an increase in local stiffness.

## Screw pullout strength with CaS/HA

Pullout tests on dynamic hip screws with and without CaS/HA were performed in order to determine if the primary fixation of a dynamic hip screw could be improved. The tests with the synthetic bone showed that an injection of CaS/HA

through both cannulated and fenestrated screws could lead to a significant increase in pullout strength. Additionally, the pullout strength in the fenestrated groups was higher than in the cannulated groups. The absolute pullout strengths recorded for the human femoral heads fell in the range of pullout strengths given by the low- and high-density blocks. Conversely, there were no significant differences between groups in the pullout tests with the human bones.

The pullout strength was greatly influenced by the spreading of the CaS/HA inside the porous bone. In the low-density blocks, injection through the cannulated screws led to a uniform spreading at the tip of the screw. Further insertion resulted in good integration between the screw and CaS/HA. Injection through the fenestrated screws led to direct incorporation of the CaS/HA in the threads of the screw and the bone directly surrounding it. Even though CaS/HA appeared to have spread more into the threads of the cannulated screws, the pullout strength was higher in the fenestrated group. This indicates that for primary stability, it is more important to have an even distribution of material around the screw rather than a large concentration at the tip. This is further supported by the results from the tests with the high-density blocks, where the fenestrated group still showed the highest pullout strength, and the cannulated group did no longer show improvement over the empty group. This indicates that osteoporotic patients could benefit more from inclusion of CaS/HA. The spreading of CaS/HA in the high-density blocks was similar to that in the low-density blocks, but the material remaining attached to the screw after pullout was different for the cannulated screws. No CaS/HA remained in the threads, indicating that no strong connection was present between CaS/HA and the screw. In the human femoral heads, injection through neither of the screws resulted in proper spreading of CaS/HA. The spreading was limited because the porous trabecular structure was filled with (coagulated) biological material. Additionally, the cannula was not closed allowing CaS/HA to flow back during injection. Without proper spreading no differences in pullout strength could be observed.

The ability of CaS/HA to stabilize orthopaedic devices has not been widely studied biomechanically. However, CaS/HA has similar initial mechanical properties as calcium phosphate (CaP) cements (Nilsson et al., 2003; Zhu et al., 2012; Ajaxon et al., 2017). Therefore, CaS/HA can be expected to perform at least equally well in applications where improved stability has been achieved with CaP. CaP was proved to be able to double the pullout strength of suture anchors in proximal humeri (Diaz et al., 2020). Similarly, in a direct comparison, CaP has been shown to increase the stability of pedicle screws to a similar degree as PMMA (Sun et al., 2020).

## In situ loading

Study VI was designed to gain more insight in the mechanical behaviour of CaS/HA after it is injected into trabecular bone. The use of synchrotron CT imaging resulted in the acquisition of images with a voxel size of only 2.75 µm. At this resolution, initiation and propagation of microcracks, and separation between trabeculae and CaS/HA could be observed. Bone is generally regarded as relatively stiff and brittle material compared to other tissues. However, by investigating the mechanical behaviour of bone at a microscale more ductile behaviour has been observed. Turunen et al. (2020) reported local strains of 6-7% before damage initiated in individual trabeculae. In study VI, the bone specimen also reached similar strains. Conversely, the CaS/HA specimen fractured well before strains of this magnitude were reached. This is well in line with mechanical properties reported for calcium sulphate dihydrate cements (Koh et al., 2014). It was therefore also not unsurprising that damage in the composite sample initiated in the CaS/HA. In the pure CaS/HA specimen the damage nearly instantaneously propagated through the full specimen. While in the composite specimen, propagation of damage was halted by the presence of bone. Instead of individual cracks propagating through the specimen, multiple microcracks initiated in this specimen, leading to higher absorbed energy.

Digital volume correlation is a useful technique that can be used to calculate displacements and strains inside a 3D volume. In this case it was used to identify regions of failure rather than to quantify, for example, strain in regions before failure. Determining strains before failure is possible with the use of smaller load steps (Turunen et al., 2020). However, decreasing the load steps increases the risk of radiation damage affecting the mechanical behaviour of the bone. With the used image settings, radiation damage was likely to occur in regions where the stacks overlapped after 5 load steps and were therefore intentionally kept relatively large (Barth et al., 2011; Pena Fernandez et al., 2018). It is advisable to perform estimated radiation dose calculations before experimental testing. Together with the knowledge at what global strain failure will occur, this allows for optimization of the load step size.

The added knowledge about the damage initiation and propagation could help to develop improved FE models of bone and CaS/HA. The data presented can best be used for models also investigating the initiation and propagation of cracks at a microscale. A simpler material formulation for the composite of CaS/HA and bone could not be determined. This was largely due to the low amount of specimens and large variation in BV/TV and penetration of CaS/HA. To obtain a material formulation that can be used for the models presented in study IV, more specimens with lower variation are required. To decrease the variation, for example, the anisotropy and BV/TV can be accounted for before acquisition of the specimens (Sas et al., 2021). New options for improving the

penetration of CaS/HA into trabecular bone should also be explored. Alternatively, an experiment could be conducted to compare the mechanical behaviour of CaS/HA and low-viscosity PMMA cements, that can fully penetrate the trabecular bone structure of cylindrical specimens (Sas et al., 2021). Through a direct comparison of the two cements and bone specimens with low-viscosity PMMA cement, a material formulation for bone and CaS/HA can potentially be derived.

## 6.2. Limitations

The main limitations in this thesis are divided in limitations regarding the studies involving mechanical testing of samples (study I, V, VI), and limitations regarding the studies including FE analyses (study II, III, IV).

### Mechanical testing

One of the limitations is the biological variation of the specimens. When studying material behaviour, test samples can often be engineered to fit the mechanical test. This option is generally not available when working with biological tissue and means that large amounts of samples are required to be able to show significant differences.

In study I, the setup was designed in such a way that all femora could be loaded under the same angles. This was fully based on the shape of the proximal femora themselves and not on realistic fall scenarios accounting for, for example, the centre of mass or motor control of the subjects. Additionally, the loading rate was set to a constant 5 mm/s, which is not in line with a realistic fall where impact occurs at speeds of approximately 3 m/s (Van Den Kroonenberg et al., 1996). This reduced speed was required to allow for strain measurements using DIC based on the framerate of the high-speed cameras.

Another limitation originating from the anatomy of the femur is the limited region that could be used for DIC on the medial and lateral side. While the anterior side is relatively flat and well suited for DIC measurements (Grassi et al., 2014), the medial and lateral side of the femoral neck are more curved. Due to this high curvature and the limited focal depth of the high-speed cameras the coverage of the regions of interest was limited. On the lateral side this limitation was even greater due to the greater trochanter occluding large parts of the neck. Since the fractures generally initiated in regions occluded by the greater trochanter, measurements of strain in these regions could not be obtained. However, this does not appear to be completely impossible. With the use of the

FE models validated in study II, it is possible to predict sites where fracture is expected to initiate. This would allow for the design of a subject-specific loading setup that enables recording of strains within the region where fracture will initiate.

The use of synthetic bone in addition to the human femoral heads in study V helped to partially account for the biological variation presented by the femoral heads. This way it was possible to show that CaS/HA can have a positive outcome on the stability of a dynamic hip screw. The inability to show differences in stability in the human femoral heads can mostly be attributed to the lack of spreading of CaS/HA. However, even with proper spreading it is not likely that significant differences could be measured. The measurements of BV/TV, insertion angle, and femoral head diameter showed correlations within the individual groups, but it was not possible to pair samples between groups based on these parameters alone. All obtained femoral heads were subcapital hip fractures extracted with an extractor screw. This led to additional variation that cannot easily be accounted for. Namely, the fracture surface, and location and depth of the hole left by the extractor screw. Since the fractures were subcapital there was not enough bone left to cut the heads in such a way that all bone affected by the fracture could be removed and that anisotropy in the femoral head could be accounted for. To be able to show significant differences with use of human femoral heads it would be better to use cadaveric femora or femoral heads obtained from total hip replacements. Erhart et al. (2011) investigated the pullout strength of the Proximal Femur Nail antirotation™ blade augmented with 4-5 ml low-viscosity PMMA cement in cadaveric human femoral heads. They showed a low significant difference ($p=0.047$) between the groups, due to large variation in pullout forces within groups (augmented: $2315.2 \pm 1060.6$ N; non-augmented: $1180.4 \pm 1171.4$ N). Clinically, PMMA and CaP bone cements have already been proven effective in the prevention of screw migration and cut-out (Matsson and Larsson, 2004; Gupta et al., 2010; Park et al., 2019). This shows that other mechanical tests should be considered to test the initial stability of fixation devices. Other options for showing screw stability are cut-out tests (Augat et al., 2002; Sermon et al., 2021). These tests replicate stance loading conditions and are used to investigate the displacement of the screw with repeated increased loads. This way migration of the screw can be better assessed However, femoral heads, with at least a part of the neck still intact, are required. This means that femoral heads from subcapital fractures and synthetic bone blocks cannot be used.

In study VI, the femoral heads obtained for study IV were used to collect multiple cylindrical specimens per head. Initially, it was planned to obtain cylindrical samples from the region where CaS/HA had already been injected. Unfortunately, while drilling, the already set CaS/HA quickly began to crumble. As alternative, the decision was made to obtain multiple specimens

from other locations in the femoral heads. From these specimens the bone marrow had to be removed before CaS/HA could be inserted. Even with all bone marrow removed, the viscosity of CaS/HA was too high to ensure filling of all space between the trabeculae. Combined, this led to specimens with high variation in bone density and spreading of CaS/HA (also within specimens). To obtain more comparable specimens, more detailed planning of the locations to drill is advised. By using, for example, µCT images of femoral heads, BV/TV and anisotropy can be accounted for (Sas et al., 2021).

## FE modelling

All FE models presented use the modulus-density relationship presented by Morgan et al. (2003). This modulus-density relationship has been used by multiple research groups and has led to accurate predictions of mechanical behaviour (Falcinelli et al., 2014; Grassi et al., 2016; Yang et al., 2018; Enns-Bray et al., 2018). However, this relationship was obtained following compression tests on trabecular samples of the femoral neck, while accounting for the physiological loading direction (Morgan et al., 2003). In the same study, other modulus-density relationships were determined for the greater trochanter, proximal tibia, and vertebrae. The authors also argued that, because the loading direction was accounted for, the modulus-density relationship may not apply for loading scenarios such as a sideways fall. Other relationships have also been shown to allow for accurate fracture strength predictions (Keyak et al., 2005; Yosibash et al., 2010; Koivumäki et al., 2012; Dall'Ara et al., 2016). Helgason et al. (2016) compared 11 relationships, and found that the relationship proposed by Morgan et al. (2003) showed one of the strongest correlations between their FE models and experimental measurements. However, they concluded that there is no one answer to what modulus-density relationship is best, since other modelling parameters and the experiments used for validation highly influence the outcome.

Similar to the modulus-density relationship, the choice for how to correct for partial volume artifacts is critical to prevent underprediction of the fracture strength when using a fracture criterion evaluating strains at the surface. Application of a minimum Young's modulus is a simple correction method, but overcorrection can lead to an overprediction the fracture strength of weaker bones. Study II therefore included a comparison of several minimum moduli, to ensure that the predicted fracture locations made sense. This shows that application of a minimum modulus, although simple, is not a robust method that can be used for all bones and multiple loading conditions. In addition to investigating the modulus-density relationship, Helgason et al. (2016) tested 5 methods to correct for partial volume artifacts. They obtained good results by removing the layer affected by artifacts in the CT images, followed by a dilation

step of the higher-density underlying bone. However, all 5 methods were based on these same principles and no conclusive answer could be given on what method was best in general.

In study III, the use of μCT images decreased the partial volume effect on the final simulations. Therefore, these models did not include any correction for these artifacts. However, not all images included calibration phantoms and the reconstruction settings varied between subjects. Since this created difficulties with consistent calibration of these images, they were calibrated directly against the clinical CT images using the grey values in the air, bone marrow, and cortical bone. Since only three points of comparison and a linear fit were used, the resulting Young's modulus was not as accurate. To achieve a better calibration between clinical CT and μCT more points should be used and other (nonlinear) relationships should be explored.

A limitation with the FE models presented in study IV were the assumed material properties of CaS/HA and bone. Although, CaS/HA has been used for multiple clinical applications (Nilsson et al., 2013), there are not many studies reporting its mechanical behaviour. In case mechanical properties are reported it is often limited to the compressive strength (Nilsson et al., 2003). Study VI was conducted to further investigate the material behaviour of CaS/HA after an injection in bone. It was found that CaS/HA has a Young's modulus of several GPa, similar to that of CaS dihydrates (Koh et al., 2014). A single Young's modulus value for the composite of CaS/HA and bone could not be determined due to the low amount of specimens and large variation in BV/TV and penetration of CaS/HA.

## 6.3. Future perspective

### Further model development and validation

As shown in this thesis, FE models are continuously improved, partly as a result of better experimental methods used for the validation experiments. One interesting follow-up on the work presented in this thesis would be to study the post-fracture behaviour. In the current FE models the simulations are stopped after the strain on the cortex has passed a pre-set limit. Including fracture behaviour of the trabecular bone and continuing the simulation after initial fracture is reached can help in determining how the damage will progress. This way it can be seen if high local strains will always lead to crack development and the severity of a potential fracture can be assessed, which could have clinical implications (Cornwall et al., 2004; Turesson et al., 2018). Fracture

mechanics based FE modelling techniques that describe the entire fracture process from crack initiation to complete fracture have recently been proposed (Gustafsson et al., 2021). These models currently use relatively simple material formulations and could be improved by including the material modelling approach presented in study II.

For the validation of models including crack progression new experiments would need to be designed. As shown in study I, a femur is likely to absorb large amounts of energy after initial failure following compression of the lateral neck. With recent developments in imaging techniques, it could be possible to develop a loading setup that could be used inside a clinical or micro CT scanner, following the recent work in single leg stance by Martelli et al. (2021). By creating a similar setup for femora loaded in a sideways fall, this could be used to perform DVC analysis to better track where fracture initiates and how it progresses.

To increase the robustness of the FE models, the modelling of the cortical bone should be improved. In the present study a lower limit for the Young's modulus of the cortex was set, which is a commonly used strategy to overcome underestimations following from partial volume artifacts in the CT images. However, in this study a different limit (2.5 GPa) was applied compared to Grassi et al. (2016), where 5 GPa was used. This change was needed because of the change in loading condition and the difference between the subjects (old women vs young men). A modelling approach that can automatically account for these differences would be a substantial improvement. One such way could be through separate mapping of material properties to the elements representing cortical bone. One such improvement was recently presented by Schileo et al. (2020). Another option could be to create separate geometries for the trabecular and the cortical bone. An accurate representation of the cortical bone can be obtained by measuring the cortical thickness and density (Treece et al., 2010). Using this method, it is also possible to identify some of the larger holes in the cortex based on clinical CT images. These could then be included in the FE models without requiring µCT scans. It can then also be further explored if the inclusion of foramina based on clinical CT scans actually improves the ability to predict the fracture strength.

These strategies can also be used to improve the FE models presented in study IV. However, a more relevant initial improvement for these models would be to find a better material model for CaS/HA and bone. The experiment from the *in situ* loading (study VI) can be extended and used to develop a new material model for CaS/HA and bone. For proper validation this should then be extended to larger sample sets and to validation using proximal femora, similar to what has previously been done for models validated with PMMA (Basafa et al., 2015).

## Toward clinical application

Regarding fracture risk prediction, the FE models presented in this work have been shown to accurately predict the fracture strength. It has already been shown that fracture strength is a good predictor for the fracture risk in other studies (Orwoll et al., 2009; Enns-Bray et al., 2019). However, for each new model, the ability to predict the fracture risk should be validated using a clinical cohort. This way it can be determined if the predicted fracture strength is actually an independent risk factor from aBMD and other factors determined with, for example, FRAX. Aside from showing that these models can better predict fracture risk, they need to be usable for clinicians. Currently, FE models still require quite some user intervention and cannot be used in a cost-efficient manner (Viceconti et al., 2018). Automatic generation of FE models from clinical CT scans is already possible (Väänänen et al., 2019). However, these models have not yet been tested for clinical use. In general, use of CT scans for screening of fracture risk is unlikely to become cost-efficient. It would be beneficial if 3D FE models could be directly created from DXA scans. This can be achieved through the use of statistical shape and appearance models, that can approximate the 3D structure and densities of a femur based on a 2D DXA scan (Väänänen et al., 2015).

Regarding fracture prevention, the work in this thesis showed that CaS/HA can improve the fracture strength of the femur, which should reduce the fracture risk. Before large scale clinical use, one question that needs to be answered is: how much increase in fracture strength is required to achieve a substantial reduction in fracture risk? Injection of bone cement is not a trivial thing, whether it is resorbable or not. As long as it is unclear how much the fracture risk decreases, it will not be clinically accepted. However, the technique is ready to be pushed towards a clinical trial. To reduce the impact of the surgery on the patient, the trial could start on patients that have already fractured one hip. In the same surgery that the fractured hip is repaired it is possible to inject CaS/HA in the contralateral, unfractured hip. This means that no additional surgery is needed. Since the increased risk of fracturing the contralateral hip is very high after an initial fracture a more drastic measure than pharmacological treatment is warranted. Follow-ups where resorption of CaS/HA and bone density distribution is tracked over time will give a good estimate of the decreased fracture risk for the patients.

For fracture repair, the small injection of 2 ml CaS/HA was shown to lead to an increase in screw stability in the synthetic bone. The first thing that needs to be overcome to improve the initial stability in human bone, is the lack of spreading of CaS/HA. The main reasons why CaS/HA did not spread in the experiment was due to the possibility for backflow through the dynamic hip screw and the coagulated tissue. An improved injection device that prevents backflow under

high pressure has already been developed. Recruitment for a clinical trial, that aims to investigate the ability of CaS/HA to improve the long-term stability of a DHS, has started (https://clinicaltrials.gov/ct2/show/NCT04498715). In this clinical trial CaS/HA is used with either local or systemic bisphosphonates to investigate bone regeneration around the screw. Regardless of whether the CaS/HA itself improves the initial stability of the screw, the newly formed bone is expected to improve screw fixation, reduce migration and improve healing outcome.

# 7. Summary and conclusions

The overall aim of the presented thesis work was to investigate new fracture strength prediction tools, and fracture prevention and repair methods. A combination of experimental and numerical studies was performed to validate finite element (FE) models and investigate orthopaedic applications of a bone cement based on calcium sulphate/hydroxyapatite (CaS/HA).

I) *Femoral fractures during a sideways fall are the result of a compressive failure of the femoral neck.* In an experimental setting proximal femora were loaded until macroscopic failure. Full-field strain measurements showed that the superolateral neck failed under compression, before macroscopic failure resulting from failure under tension on the medial side of the femoral neck.

II) *A new benchmark for validation of FE models was set by using digital image correlation for bilateral strain measurements on a proximal femur*. This validation process highlighted the complexity of measured strain fields and difficulties of accurately predicting strains in areas with high surface irregularity.

III) *FE models including foramina can improve the accuracy of the predicted strains.* These FE models also confirmed that foramina can lead to high strains that not necessarily lead to global failure. Therefore, the inclusion of foramina is not likely to be necessary when prediction of the fracture strength is the goal.

IV) *An injection of CaS/HA in the femoral neck can increase the fracture strength of the femur.* FE models that simulated a variation in injected CaS/HA location, volume, and stiffness were created. The most substantial increase in fracture strength was achieved by optimizing the location of the injection to the lateral side of the neck.

V) *An injection of CaS/HA has the potential to improve the initial fixation of a dynamic hip screw.* Pullout tests were performed on dynamic hip screws using synthetic and human bone, with or

without CaS/HA. In synthetic bone, where CaS/HA can easily spread, significant increases in pullout strength were found. In human bone CaS/HA could not spread easily, so when considering the use of CaS/HA for clinical application special attention needs to be focused on the injection method to ensure proper spreading.

VI) *CaS/HA can strengthen trabecular bone and greatly increase its ability to absorb energy while keeping the bone largely intact.* Bone and CaS/HA samples were imaged using high-resolution X-ray tomography and loaded *in situ*. In samples containing both bone and CaS/HA, separation between bone and CaS/HA and microcracking in the CaS/HA was observed before damage to the bone became visible. The bone prevented the more brittle CaS/HA from developing large cracks leading to high energy absorption.

# 8. References


Abramo, A., Geijer, M., Kopylov, P., Ta, M., 2009. Osteotomy of Distal Radius Fracture Malunion Using a Fast Remodeling Bone Substitute Consisting of Calcium Sulphate and Calcium Phosphate. J. Biomed. Mater. Res. - Part B Appl. Biomater. 281–286. https://doi.org/10.1002/jbm.b.31524

Ajaxon, I., Acciaioli, A., Lionello, G., Ginebra, M.P., Öhman-Mägi, C., Baleani, M., Persson, C., 2017. Elastic properties and strain-to-crack-initiation of calcium phosphate bone cements: Revelations of a high-resolution measurement technique. J. Mech. Behav. Biomed. Mater. 74, 428–437. https://doi.org/10.1016/j.jmbbm.2017.06.023

Albrektsson, T., Johansson, C., 2001. Osteoinduction, osteoconduction and osseointegration. Eur. Spine J. 10, S96–S101. https://doi.org/10.1007/s005860100282

Augat, P., Rapp, S., Claes, L., 2002. A modified hip screw incorporating injected cement for the fixation of osteoporotic trochanteric fractures. J. Orthop. Trauma 16, 311–316. https://doi.org/10.1097/00005131-200205000-00004

Backman, S., 1957. The proximal end of the femur: investigations with special reference to the etiology of femoral neck fractures; anatomical studies; roentgen projections; theoretical stress calculations; experimental production of fractures. Acta Radiol. Suppl. 1–166.

Bahaloo, H., Enns-Bray, W.S., Fleps, I., Ariza, O., Gilchrist, S., Soyka, R.W., Guy, P., Palsson, H., Ferguson, S.J., Cripton, P.A., Helgason, B., 2018. On the Failure Initiation in the Proximal Human Femur Under Simulated Sideways Fall. Ann. Biomed. Eng. 46, 270–283. https://doi.org/10.1007/s10439-017-1952-z

Barrionuevo, P., Kapoor, E., Asi, N., Alahdab, F., Mohammed, K., Benkhadra, K., Almasri, J., Farah, W., Sarigianni, M., Muthusamy, K., Al Nofal, A., Haydour, Q., Wang, Z., Murad, M.H., 2019. Efficacy of pharmacological therapies for the prevention of fractures in postmenopausal women: A network meta-analysis. J. Clin. Endocrinol. Metab. 104, 1623–1630. https://doi.org/10.1210/jc.2019-00192

Barth, H.D., Zimmermann, E.A., Schaible, E., Tang, S.Y., Alliston, T., Ritchie, R.O., 2011. Characterization of the effects of x-ray irradiation on the hierarchical structure and mechanical properties of human cortical bone. Biomaterials 32, 8892–8904. https://doi.org/10.1016/j.biomaterials.2011.08.013

Basafa, E., Armiger, R.S., Kutzer, M.D., Belkoff, S.M., Mears, S.C., Armand, M., 2013. Patient-specific finite element modeling for femoral bone augmentation. Med. Eng. Phys. 35, 860–865. https://doi.org/10.1016/j.medengphy.2013.01.003

Basafa, E., Murphy, R.J., Otake, Y., Kutzer, M.D., Belkoff, S.M., Mears, S.C., Armand, M., 2015. Subject-specific planning of femoroplasty: An experimental verification study. J. Biomech. 48, 59–64. https://doi.org/10.1016/j.jbiomech.2014.11.002

Bay, B.K., Smith, T.S., Fyhrie, D.P., Saad, M., 1999. Digital volume correlation: Three-dimensional strain mapping using x-ray tomography. Exp. Mech. 39, 217–226. https://doi.org/10.1007/BF02323555

Bayraktar, H.H., Morgan, E.F., Niebur, G.L., Morris, G.E., Wong, E.K., Keaveny, T.M., 2004. Comparison of the elastic and yield properties of human femoral trabecular and cortical bone tissue. J. Biomech. 37, 27–35. https://doi.org/10.1016/S0021-9290(03)00257-4

Beckmann, J., Ferguson, S.J., Gebauer, M., Luering, C., Gasser, B., Heini, P., 2007. Femoroplasty - augmentation of the proximal femur with a composite bone cement - feasibility, biomechanical properties and osteosynthesis potential. Med. Eng. Phys. 29, 755–764. https://doi.org/10.1016/j.medengphy.2006.08.006

Belda, R., Palomar, M., Peris-Serra, J.L., Vercher-Martínez, A., Giner, E., 2020. Compression failure characterization of cancellous bone combining experimental testing, digital image correlation and finite element modeling. Int. J. Mech. Sci. 165, 105213. https://doi.org/10.1016/j.ijmecsci.2019.105213

Berry, S.D., Miller, R.R., 2008. Falls: Epidemiology, pathophysiology, and relationship to fracture. Curr. Osteoporos. Rep. 6, 149–154. https://doi.org/10.1007/s11914-008-0026-4

Berry, S.D., Samelson, E.J., Hannan, M.T., McLean, R.R., Lu, M., Adrienne Cupples, L., Shaffer, M.L., Beiser, A.L., Kelly-Hayes, M., Kiel, D.P., 2007. Second Hip Fracture in Older Men and Women The Framingham Study. Arch. Intern. Med. 167, 1971–1976. https://doi.org/10.1001/archinte.167.18.1971

Borgström, F., Karlsson, L., Ortsäter, G., Norton, N., Halbout, P., Cooper, C., Lorentzon, M., McCloskey, E. V., Harvey, N.C., Javaid, M.K., Kanis, J.A., Reginster, J.Y., Ferrari, S., 2020. Fragility fractures in Europe: burden, management and opportunities. Arch. Osteoporos. 15. https://doi.org/10.1007/s11657-020-0706-y

Brekelmans, W.A.M., Poort, H.W., Slooff, T.J.J.H., 1972. Acta Orthopaedica Scandinavica A New Method to Analyse the Mechanical Behaviour of Skeletal Parts. Acta Orthop. Scand. 43, 301–317. https://doi.org/10.3109/17453677208998949

Bukata, S. V., Crawford, B.M., Vallera, C., 2021. Orthopedic aspects of osteoporosis. Marcus Feldman's Osteoporos. 1613–1625. https://doi.org/10.1016/b978-0-12-813073-5.00067-8

Burg, K.J.L., Porter, S., Kellam, J.F., 2000. Biomaterial developments for bone tissue engineering. Biomaterials 21, 2347–2359. https://doi.org/10.1016/S0142-9612(00)00102-2

Burr, D.B., 2019. Changes in bone matrix properties with aging. Bone 120, 85–93. https://doi.org/10.1016/j.bone.2018.10.010

Carter, D.R., Hayes, W.C., 1976. Bone compressive strength the influence of density and strain rate. Science (80-. ). 194, 1174–1176. https://doi.org/10.1126/science.996549

Carter, D.R., Hayes, W.C., 1977. The compressive behavior of bone as a two-phase porous structure. J. Bone Jt. Surg. 59-A, 954–962. https://doi.org/10.1007/978-1-4471-5451-8_116

Charnley, J., 1961. Hemiarthroplasty of the hip. Lancet 1129–1132.

Cornwall, R., Gilbert, M.S., Koval, K.J., Strauss, E., Siu, A.L., 2004. Functional Outcomes and Mortality Vary among Different Types of Hip Fractures A Function of Patient Characteristics. Clin. Orthop. Relat. Res. 64–71. https://doi.org/10.1097/01.blo.0000132406.37763.b3

Cristofolini, L., Juszczyk, M., Martelli, S., Taddei, F., Viceconti, M., 2007. In vitro replication of spontaneous fractures of the proximal human femur. J. Biomech. 40, 2837–2845. https://doi.org/10.1016/j.jbiomech.2007.03.015

Cummings, S.R., Martin, J.S., McClung, M.R., Siris, E.S., Eastell, R., Reid, I.R., Delmas, P., Zoog, H.B., Austin, M., Wang, A., Kutilek, S., Adami, S., Zanchetta, J., Libanati, C., Siddhanti, S., Christiansen, C., 2009. Denosumab for Prevention of Fractures in Postmenopausal Women with Osteoporosis. N. Engl. J. Med. 361, 756–765. https://doi.org/10.1056/NEJMoa0809493

Dall'Ara, E., Luisier, B., Schmidt, R., Kainberger, F., Zysset, P., Pahr, D., 2013. A nonlinear QCT-based finite element model validation study for the human femur tested in two configurations in vitro. Bone 52, 27–38. https://doi.org/10.1016/j.bone.2012.09.006

Danesi, V., Tozzi, G., Cristofolini, L., 2016. Application of digital volume correlation to study the efficacy of prophylactic vertebral augmentation. Clin. Biomech. 39, 14–24. https://doi.org/10.1016/j.clinbiomech.2016.07.010

De Bakker, P.M., Manske, S.L., Ebacher, V., Oxland, T.R., Cripton, P.A., Guy, P., 2009. During sideways falls proximal femur fractures initiate in the superolateral cortex: Evidence from high-speed video of simulated fractures. J. Biomech. 42, 1917–1925. https://doi.org/10.1016/j.jbiomech.2009.05.001

Dempster, D.W., Marcus, R., Bouxsein, M.L., 2021. The Nature of Osteoporosis, Marcus and Feldman's Osteoporosis. INC. https://doi.org/10.1016/B978-0-12-415853-5.00002-9

Diaz, M.A., Branch, E.A., Paredes, L.A., Oakley, E., Baker, C.E., 2020. Calcium Phosphate Bone Void Filler Increases Threaded Suture Anchor Pullout Strength: A Biomechanical Study. Arthrosc. J. Arthrosc. Relat. Surg. https://doi.org/10.1016/j.arthro.2019.12.003

DiPisa, J., 1975. An investigation of the temperature problem at the bone-acrylic cement interface of the total hip replacement. Lehigh Preserv. Institutional Repos. Lehigh University.

Dyer, S.M., Crotty, M., Fairhall, N., Magaziner, J., Beaupre, L.A., Cameron, I.D., Sherrington, C., 2016. A critical review of the long-term disability outcomes following hip fracture. BMC Geriatr. 16, 1–18. https://doi.org/10.1186/s12877-016-0332-0

Ekström, W., Miedel, R., Ponzer, S., Hedström, M., Samnegård, E., Tidermark, J., 2009. Quality of life after a stable trochanteric fracture--a prospective cohort study on 148 patients. J. Orthop. Trauma 23, 39–44. https://doi.org/10.1097/BOT.0b013e318191f5e4

Enns-Bray, W.S., Bahaloo, H., Fleps, I., Ariza, O., Gilchrist, S., Widmer, R., Guy, P., Pálsson, H., Ferguson, S.J., Cripton, P.A., Helgason, B., 2018. Material mapping strategy to improve the predicted response of the proximal femur to a sideways fall impact. J. Mech. Behav. Biomed. Mater. 78, 196–205. https://doi.org/10.1016/j.jmbbm.2017.10.033

Enns-Bray, W.S., Bahaloo, H., Fleps, I., Pauchard, Y., Taghizadeh, E., Sigurdsson, S., Aspelund, T., Büchler, P., Harris, T., Gudnason, V., Ferguson, S.J., Pálsson, H., Helgason, B., 2019. Biofidelic finite element models for accurately classifying hip fracture in a retrospective clinical study of elderly women from the AGES Reykjavik cohort. Bone 120, 25–37. https://doi.org/10.1016/j.bone.2018.09.014

Erhart, S., Schmoelz, W., Blauth, M., Lenich, A., 2011. Biomechanical effect of bone cement augmentation on rotational stability and pull-out strength of the Proximal Femur Nail Antirotation. Injury 42, 1322–1327. https://doi.org/10.1016/j.injury.2011.04.010

Eriksson, F., Mattsson, P., Larsson, S., 2002. The Effect of Augmentation With Resorbable or Conventional Bone Cement on the Holding Strength for Femoral Neck Fracture Devices. J. Orthop. Trauma 16, 302–310. https://doi.org/10.1097/00005131-200205000-00003

Falcinelli, C., Schileo, E., Balistreri, L., Baruffaldi, F., Bordini, B., Viceconti, M., Albisinni, U., Ceccarelli, F., Milandri, L., Toni, A., Taddei, F., 2014. Multiple loading conditions analysis can improve the association between finite element bone strength estimates and proximal femur fractures: A preliminary study in elderly women. Bone 67, 71–80. https://doi.org/10.1016/j.bone.2014.06.038

Faulkner, R., Bailey, D., 2007. Osteoporosis: A Pediatric Concern?, in: Medicine and Sport Science. pp. 1–12. https://doi.org/10.1159/000102993

Ferrari, S., Reginster, J.-Y., Brandi, M.L., Kanis, J.A., Devogelaer, J.-P., Kaufman, J.-M., Féron, J.-M., Kurth, A., Rizzoli, R., 2016. Unmet needs and current and future approaches for osteoporotic patients at high risk of hip fracture. Arch. Osteoporos. 11, 37. https://doi.org/10.1007/s11657-016-0292-1

Fleps, I., Fung, A., Guy, P., Ferguson, S.J., Helgason, B., Cripton, P.A., 2019. Subject-specific ex vivo simulations for hip fracture risk assessment in sideways falls. Bone 125, 36–45. https://doi.org/10.1016/j.bone.2019.05.004

Fox, K.M., Magaziner, J., Hebel, J.R., Kenzora, J.E., Kashner, T.M., 1999. Intertrochanteric versus femoral neck hip fractures: Differential characteristics, treatment, and sequelae. Journals Gerontol. - Ser. A Biol. Sci. Med. Sci. 54, 635–640. https://doi.org/10.1093/gerona/54.12.M635

Galibert, P., Deramond, H., Rosat, P., Le Gars, D., 1987. Preliminary note on the treatment of vertebral angioma by percutaneous acrylic vertebroplasty. Neurochirurgie. 33, 166–168.

Geusens, P., Milisen, K., Dejaeger, E., Boonen, S., 2003. Falls and Fractures in Postmenopausal Women: A Review. Br. Menopause Soc. J. 9, 101–106. https://doi.org/10.1177/136218070300900307

Gilchrist, S., Guy, P., Cripton, P.A., 2013. Development of an Inertia-Driven Model of Sideways Fall for Detailed Study of Femur Fracture Mechanics. J. Biomech. Eng. 135, 121001. https://doi.org/10.1115/1.4025390

Grassi, L., Schileo, E., Taddei, F., Zani, L., Juszczyk, M., Cristofolini, L., Viceconti, M., 2012. Accuracy of finite element predictions in sideways load configurations for the proximal human femur. J. Biomech. 45, 394–399. https://doi.org/10.1016/j.jbiomech.2011.10.019

Grassi, L., Isaksson, H., 2015. Extracting accurate strain measurements in bone mechanics: a critical review of current methods. J. Mech. Behav. Biomed. Mater. 50, 43–54. https://doi.org/doi:10.1016/j.jmbbm.2015.06.006

Grassi, L., Väänänen, S.P., Amin Yavari, S., Weinans, H., Jurvelin, J.S., Zadpoor, A. a., Isaksson, H., 2013. Experimental Validation Of Finite Element Model For Proximal Composite Femur Using Optical Measurements. J. Mech. Behav. Biomed. Mater. 21, 86–94. https://doi.org/10.1016/j.jmbbm.2013.02.006

Grassi, L., Väänänen, S.P., Ristinmaa, M., Jurvelin, J.S., Isaksson, H., 2016. How accurately can subject-specific finite element models predict strains and strength of human femora? Investigation using full-field measurements. J. Biomech. 49, 802–806. https://doi.org/10.1016/j.jbiomech.2016.02.032

Grassi, L., Väänänen, S.P., Amin Yavari, S., Jurvelin, J.S., Weinans, H., Ristinmaa, M., Zadpoor, A.A., Isaksson, H., 2014. Full-field Strain Measurement During Mechanical Testing of the Human Femur at Physiologically Relevant Strain Rates. J. Biomech. Eng. 136. https://doi.org/10.1115/1.4028415

Greenspan, S.L., Myers, E.R., Kiel, D.P., Parker, R.A., Hayes, W.C., Resnick, N.M., 1998. Fall direction, bone mineral density, and function: Risk factors for hip fracture in frail nursing home elderly. Am. J. Med. 104, 539–545. https://doi.org/10.1016/S0002-9343(98)00115-6

Gupta, R.K., Gupta, V., Gupta, N., 2012. Outcomes of osteoporotic trochanteric fractures treated with cement-augmented dynamic hip screw. Indian J. Orthop. 46, 640–645. https://doi.org/10.4103/0019-5413.104193

Gustafsson, A., Tognini, M., Bengtsson, F., Gasser, T.C., Isaksson, H., Grassi, L., 2021. Subject-specific FE models of the human femur predict fracture path and bone strength under single-leg-stance loading. J. Mech. Behav. Biomed. Mater. 113, 104118. https://doi.org/10.1016/j.jmbbm.2020.104118

Harrington, K.D., Franklin, S.H., Enis, J.E., Johnston, J.O., Dick, H.M., Gristina, A.G., 1976. Methylmethacrylate as an Adjunct in Internal Fixation of Pathological Fractures. J. Bone Jt. Surg. 58, 1047–1055.

Harvey, L., Mitchell, R., Brodaty, H., Draper, B., Close, J., 2016. Differing trends in fall-related fracture and non-fracture injuries in older people with and without dementia. Arch. Gerontol. Geriatr. 67, 61–67. https://doi.org/10.1016/j.archger.2016.06.014

Hatten Jr, H.P., Voor, M.J., 2012. bone healing using a bi-Phasic Ceramic bone Substitute demonstrated in human Vertebroplasty and with histology in a Rabbit Cancellous bone defect Model, Interventional Neuroradiology.

Heini, P.F., Franz, T., Fankhauser, C., Gasser, B., Ganz, R., 2004. Femoroplasty-augmentation of mechanical properties in the osteoporotic proximal femur: A biomechanical investigation of PMMA reinforcement in cadaver bones. Clin. Biomech. 19, 506–512. https://doi.org/10.1016/j.clinbiomech.2004.01.014

Helgason, B., Gilchrist, S., Ariza, O., Vogt, P., Enns-Bray, W., Widmer, R.P., Fitze, T., Pálsson, H., Pauchard, Y., Guy, P., Ferguson, S.J., Cripton, P.A., 2016. The influence of the modulus-density relationship and the material mapping method on the simulated mechanical response of the proximal femur in side-ways fall loading configuration. Med. Eng. Phys. 38, 679–689. https://doi.org/10.1016/j.medengphy.2016.03.006

Helgason, B., S.Gilchrist, Ariza, O., Chak, J.D., Zheng, G., Widmer, R.P., Ferguson, S.J., Guy, P., Cripton, P.A., 2014. Development of a balanced experimental-computational approach to understanding the mechanics of proximal femur fractures. Med. Eng. Phys. 36, 793–799. https://doi.org/10.1016/j.medengphy.2014.02.019

Helgason, B., Taddei, F., Pálsson, H., Schileo, E., Cristofolini, L., Viceconti, M., Brynjólfsson, S., 2008. A modified method for assigning material properties to FE models of bones. Med. Eng. Phys. 30, 444–453. https://doi.org/10.1016/j.medengphy.2007.05.006

Hernlund, E., Svedbom, A., Ivergård, M., Compston, J., Cooper, C., Stenmark, J., McCloskey, E. V., Jönsson, B., Kanis, J.A., 2013. Osteoporosis in the European Union: Medical management, epidemiology and economic burden: A report prepared in collaboration with the International Osteoporosis Foundation (IOF) and the European Federation of Pharmaceutical Industry Associations (EFPIA). Arch. Osteoporos. 8. https://doi.org/10.1007/s11657-013-0136-1

Huiskes, R., Chao, E.Y.S., 1983. A survey of finite element analysis in orthopedic biomechanics: The first decade. J. Biomech. 16, 385–409. https://doi.org/10.1016/0021-9290(83)90072-6

Huiskes, R., Janssen, J.D., Slooff, T.J., 1983. A detailed comparison of experimental and theoretical stress-analysis of a human femur. Mech. Prop. bone 45, 211–234.

Hussein, A.I., Barbone, P.E., Morgan, E.F., 2012. Digital volume correlation for study of the mechanics of whole bones. Procedia IUTAM 4, 116–125. https://doi.org/10.1016/j.piutam.2012.05.013

Järvinen, T.L.N., Michaëlsson, K., Jokihaara, J., Collins, G.S., Perry, T.L., Mintzes, B., Musini, V., Erviti, J., Gorricho, J., Wright, J.M., Sievänen, H., 2015. Overdiagnosis of bone fragility in the quest to prevent hip fracture. BMJ 350, h2088. https://doi.org/10.1136/bmj.h2088

Jha, S., Wang, Z., Laucis, N., Bhattacharyya, T., 2015. Trends in Media Reports, Oral Bisphosphonate Prescriptions, and Hip Fractures 1996-2012: An Ecological Analysis. J. Bone Miner. Res. 30, 2179–2187. https://doi.org/10.1002/jbmr.2565

Jiang, J., Yang, C. hui, Lin, Q., Yun, X. dong, Xia, Y. yi, 2015. Does Arthroplasty Provide Better Outcomes Than Internal Fixation At Mid- and Long-term Followup? A Meta-analysis. Clin. Orthop. Relat. Res. 473, 2672–2679. https://doi.org/10.1007/s11999-015-4345-3

Johannesdottir, F., Allaire, B., Bouxsein, M.L., 2018. Fracture Prediction by Computed Tomography and Finite Element Analysis : Current and Future Perspectives. Curr. Osteoporos. Rep. 16, 411–422. https://doi.org/10.1007/s11914-018-0450-z

Johannesdottir, F., Thrall, E., Muller, J., Keaveny, T.M., Kopperdahl, D.L., Bouxsein, M.L., 2017. Comparison of non-invasive assessments of strength of the proximal femur. Bone 105, 93–102. https://doi.org/10.1016/j.bone.2017.07.023

Kanis, J.A., Johansson, H., Harvey, N.C., McCloskey, E. V., 2018. A brief history of FRAX. Arch. Osteoporos. 13. https://doi.org/10.1007/s11657-018-0510-0

Kanis, J.A., Oden, A., Johansson, H., Borgström, F., Ström, O., McCloskey, E., 2009. FRAX® and its applications to clinical practice. Bone 44, 734–743. https://doi.org/10.1016/j.bone.2009.01.373

Kannus, P., Parkkari, J., Niemi, S., Palvanen, M., 1996. Epidemiology of osteoporotic ankle fractures in elderly persons in Finland. Ann. Intern. Med. 125, 975–978. https://doi.org/10.7326/0003-4819-125-12-199612150-00007

Karlsson, M.K., Rosengren, B.E., 2020. Exercise and Peak Bone Mass. Curr. Osteoporos. Rep. 18, 285–290. https://doi.org/10.1007/s11914-020-00588-1

Kasra, M., Grynpas, M.D., 2007. On shear properties of trabecular bone under torsional loading: Effects of bone marrow and strain rate. J. Biomech. 40, 2898–2903. https://doi.org/10.1016/j.jbiomech.2007.03.008

Katz, Y., Yosibash, Z., 2020. New insights on the proximal femur biomechanics using Digital Image Correlation. J. Biomech. 101, 109599. https://doi.org/10.1016/J.JBIOMECH.2020.109599

Keyak, J.H., Kaneko, T.S., Tehranzadeh, J., Skinner, H.B., 2005. Predicting proximal femoral strength using structural engineering models. Clin. Orthop. Relat. Res. 219–228. https://doi.org/10.1097/01.blo.0000164400.37905.22

Keyak, J.H., Rossi, S. a, Jones, K. a, Skinner, H.B., 1997. Prediction of Femoral Fracture Load using Automated Finite Element Modelling. J Biomech 31, 125–133. https://doi.org/10.1016/S0021-9290(97)00123-1

Knaack, D., Goad, M.E.P., Aiolova, M., Rey, C., Tofighi, A., Chakravarthy, P., Lee, D.D., 1998. Resorbable Calcium Phosphate Bone Substitute, Inc. J Biomed Mater Res (Appl Biomater). John Wiley & Sons.

Koh, I., Lopez, A., Helgason, B., Ferguson, S.J., 2014. The compressive modulus and strength of saturated calcium sulphate dihydrate cements : Implications for testing standards. J. Mech. Behav. Biomed. Mater. 34, 187–198. https://doi.org/10.1016/j.jmbbm.2014.01.018

Koivumäki, J.E.M., Thevenot, J., Pulkkinen, P., Kuhn, V., Link, T.M., Eckstein, F., Jämsä, T., 2012. Ct-based finite element models can be used to estimate experimentally measured failure loads in the proximal femur. Bone 50, 824–829. https://doi.org/10.1016/j.bone.2012.01.012

Kontulainen, S.A., Johnston, J.D., 2021. Physical activity, exercise, and skeletal health, Marcus and Feldman's Osteoporosis. INC. https://doi.org/10.1016/b978-0-12-813073-5.00022-8

Levy, H., Seydafkan, S., Rice, J.D., Easley, K.A., Tangpricha, V., 2012. Comparative efficacy of vertebroplasty, kyphoplasty, and medical therapy for vertebral fractures on survival and prevention of recurrent fractures. Endocr. Pract. 18, 499–507. https://doi.org/10.4158/EP11349.OR

Lin, W.C., Cheng, T.T., Lee, Y.C., Wang, T.N., Cheng, Y.F., Lui, C.C., Yu, C.Y., 2008. New Vertebral Osteoporotic Compression Fractures after Percutaneous Vertebroplasty: Retrospective Analysis of Risk Factors. J. Vasc. Interv. Radiol. 19, 225–231. https://doi.org/10.1016/j.jvir.2007.09.008

Lin, W.C., Lee, Y.C., Lee, C.H., Kuo, Y.L., Cheng, Y.F., Lui, C.C., Cheng, T.T., 2008. Refractures in cemented vertebrae after percutaneous vertebroplasty: A retrospective analysis. Eur. Spine J. 17, 592–599. https://doi.org/10.1007/s00586-007-0564-y

Lotz, J.C., Cheal, E.J., Hayes, W.C., 1991. Fracture prediction for the proximal femur using finite element models Part I--Linear analysis-annotated. J. Biomech. Eng. 113, 353–360.

Lowe, J.A., Crist, B.D., Bhandari, M., Ferguson, T.A., 2010. Optimal Treatment of Femoral Neck Fractures According to Patient's Physiologic Age: An Evidence-Based Review. Orthop. Clin. North Am. 41, 157–166. https://doi.org/10.1016/j.ocl.2010.01.001

Martelli, S., Giorgi, M., Dall' Ara, E., Perilli, E., 2021. Damage tolerance and toughness of elderly human femora. Acta Biomater. 123, 167–177. https://doi.org/10.1016/j.actbio.2021.01.011

Mattsson, P., Larsson, S., 2004. Unstable trochanteric fractures augmented with calcium phosphate cement. A prospective randomized study using radiostereometry to measure fracture stability. Scand. J. Surg. 93, 223–228.

McCloskey, E., Rathi, J., Heijmans, S., Blagden, M., Cortet, B., Czerwinski, E., Hadji, P., Payer, J., Palmer, K., Stad, R., Papapoulos, S., McCloskey EVMcCloskey, E., 2020. The osteoporosis treatment gap in patients at risk of fracture in European primary care: a multi-country cross-sectional observational study. Osteoporos. Int. 32, 251–259. https://doi.org/10.1007/s00198-020-05557-z

McClung, M.R., Wagman, R.B., Miller, P.D., Wang, A., Lewiecki, E.M., 2017. Observations following discontinuation of long-term denosumab therapy. Osteoporos. Int. 28, 1723–1732. https://doi.org/10.1007/s00198-017-3919-1

Mei, J., Quan, K., Wang, H., Dai, Y., Zhang, F., Ni, M., 2019. Total cross-sectional area of the femoral neck nutrient foramina measured to assess arterial vascular beds in the femoral head. J. Orthop. Surg. Res. 14, 1–7. https://doi.org/10.1186/s13018-019-1480-7

Mendes, M.M., Sahni, S., 2021. Calcium and vitamin D in the management of osteoporosis, Marcus and Feldman's Osteoporosis. INC. https://doi.org/10.1016/b978-0-12-813073-5.00070-8

Morgan, E.F., Bayraktar, H.H., Keaveny, T.M., 2003. Trabecular bone modulus-density relationships depend on anatomic site. J. Biomech. 36, 897–904. https://doi.org/10.1016/S0021-9290(03)00071-X

Nawathe, S., Akhlaghpour, H., Bouxsein, M.L., Keaveny, T.M., 2014. Microstructural failure mechanisms in the human proximal femur for sideways fall loading. J. Bone Miner. Res. 29, 507–515. https://doi.org/10.1002/jbmr.2033

Neuman, M.D., Silber, J.H., Magaziner, J.S., Passarella, M.A., Mehta, S., Werner, R.M., 2014. Survival and functional outcomes after hip fracture among nursing home residents. JAMA Intern. Med. 174, 1273–1280. https://doi.org/10.1001/jamainternmed.2014.2362

Nilsson, M., Wielanek, L., Wang, J.S., Tanner, K.E., Lidgren, L., 2003. Factors influencing the compressive strength of an injectable calcium sulfate-hydroxyapatite cement. J. Mater. Sci. Mater. Med. 14, 399–404. https://doi.org/10.1023/A:1023254632704

Nilsson, M., Zheng, M.H., Tägil, M., 2013. The composite of hydroxyapatite and calcium sulphate: A review of preclinical evaluation and clinical applications. Expert Rev. Med. Devices. https://doi.org/10.1586/17434440.2013.827529

Oñativia, I.J., Slulittel, P.A.I., Dilernia, F.D., Viezcas, J.M.G., Vietto, V., Ramkumar, P.N., Buttaro, M.A., Piuzzi, N.S., 2018. Outcomes of nondisplaced intracapsular femoral neck fractures with internal screw fixation in elderly patients: a systematic review. HIP Int. 28, 24–26. https://doi.org/10.5301/hipint.5000532

Op Den Buijs, J., Dragomir-Daescu, D., 2011. Validated finite element models of the proximal femur using two-dimensional projected geometry and bone density. Comput. Methods Programs Biomed. 104, 168–174. https://doi.org/10.1016/j.cmpb.2010.11.008

Orwoll, E.S., Marshall, L.M., Nielson, C.M., Cummings, S.R., Lapidus, J., Cauley, J.A., Ensrud, K., Lane, N., Hoffmann, P.R., Kopperdahl, D.L., Keaveny, T.M., 2009. Finite Element Analysis of the Proximal Femur and Hip Fracture Risk in Older Men. J. Bone Miner. Res. 24, 475–483. https://doi.org/10.1359/jbmr.081201

Palanca, M., Tozzi, G., Cristofolini, L., 2015. The use of digital image correlation in the biomechanical area: a review. Int. Biomech. 3, 1–21. https://doi.org/10.1080/23335432.2015.1117395

Park, J., Shin, J.M., Lee, D.K., Lee, S., Paik, S.H., Lee, B.H., 2019. The Effect of Synthetic Osteoconductive Bone Graft Material for Augmentation of Internally Fixed Unstable Trochanteric Fractures. Biomed Res. Int. 2019. https://doi.org/10.1155/2019/5879089

Parkkari, J., Kannus, P., Palvanen, M., Natri, A., Vainio, J., Aho, H., Vuori, I., Ja, M., 1999. Clinical Investigations Majority of Hip Fractures Occur as a Result of a Fall and Impact on the Greater Trochanter of the Femur : A Prospective Controlled Hip Fracture Study with 206 Consecutive Patients. Calcif. Tissue Int. 183–187.

Pasco E Seeman M J Henry E N Merriman G C Nicholson M A Kotowicz, J.A., 2006. The population burden of fractures originates in women with osteopenia, not osteoporosis. Osteoporos Int 17, 1404–1409. https://doi.org/10.1007/s00198-006-0135-9

Peña Fernández, M., Cipiccia, S., Dall'Ara, E., Bodey, A.J., Parwani, R., Pani, M., Blunn, G.W., Barber, A.H., Tozzi, G., 2018. Effect of SR-microCT radiation on the mechanical integrity of trabecular bone using in situ mechanical testing and digital volume correlation. J. Mech. Behav. Biomed. Mater. 88, 109–119. https://doi.org/10.1016/j.jmbbm.2018.08.012

Raina, D.B., Isaksson, H., Hettwer, W., Kumar, A., Lidgren, L., Tägil, M., 2016. A Biphasic Calcium Sulphate/Hydroxyapatite Carrier Containing Bone Morphogenic Protein-2 and Zoledronic Acid Generates Bone. Sci. Rep. 6, 26033. https://doi.org/10.1038/srep26033

Raina, D.B., Liu, Y., Isaksson, H., Tägil, M., Lidgren, L., 2019. Synthetic hydroxyapatite: a recruiting platform for biologically active molecules. Acta Orthop. 91, 126–132. https://doi.org/10.1080/17453674.2019.1686865

Reilly, D.T., Burstein, A.H., Frankel, V.H., 1974. The elastic modulus for bone. J. Biomech. 7. https://doi.org/10.1016/0021-9290(74)90018-9

Reilly, D.T., Burstein, A.H., 1975. The elastic and ultimate properties of compact bone tissue. J Biomech 8, 393–405. https://doi.org/10.1016/0021-9290(75)90075-5

Reznikov, N., Bilton, M., Lari, L., Stevens, M.M., Kröger, R., 2018. Fractal-like hierarchical organization of bone begins at the nanoscale. Science (80-. ). 360, eaao2189. https://doi.org/10.1126/science.aao2189

Saita, Y., Ishijima, M., Kaneko, K., 2015. Atypical femoral fractures and bisphosphonate use : current evidence and clinical implications. Ther. Adv. Chronic Dis. 6, 185–193. https://doi.org/10.1177/2040622315584114

Sandhu, S.K., Nguyen, N.D., Center, J.R., Pocock, N.A., Eisman, J.A., Nguyen, T. V., 2010. Prognosis of fracture: Evaluation of predictive accuracy of the FRAX™ algorithm and Garvan nomogram. Osteoporos. Int. 21, 863–871. https://doi.org/10.1007/s00198-009-1026-7

Sas, A., Helgason, B., Ferguson, S.J., van Lenthe, G.H., 2021. Mechanical and morphological characterization of PMMA/bone composites in human femoral heads. J. Mech. Behav. Biomed. Mater. 115, 104247. https://doi.org/10.1016/j.jmbbm.2020.104247

Schileo, E., Balistreri, L., Grassi, L., Cristofolini, L., Taddei, F., 2014. To what extent can linear finite element models of human femora predict failure under stance and fall loading configurations? J. Biomech. 47, 3531–3538. https://doi.org/10.1016/j.jbiomech.2014.08.024

Schileo, E., Pitocchi, J., Falcinelli, C., Taddei, F., 2020. Cortical bone mapping improves finite element strain prediction accuracy at the proximal femur. Bone 136, 115348. https://doi.org/10.1016/j.bone.2020.115348

Schileo, E., Taddei, F., Cristofolini, L., Viceconti, M., 2008. Subject-specific finite element models implementing a maximum principal strain criterion are able to estimate failure risk and fracture location on human femurs tested in vitro. J. Biomech. 41, 356–367. https://doi.org/10.1016/j.jbiomech.2007.09.009

Sermon, A., Zderic, I., Khatchadourian, R., Scherrer, S., Knobe, M., Stoffel, K., Gueorguiev, B., 2021. Bone cement augmentation of femoral nail head elements increases their cut-out resistance in poor bone quality– A biomechanical study. J. Biomech. 118, 110301. https://doi.org/10.1016/j.jbiomech.2021.110301

Shumway-Cook, A., Brauer, S., Woollacott, M., 2000. Predicting the probability for falls in community-dwelling older adults using the timed up and go test. Phys. Ther. 80, 896–903. https://doi.org/10.1093/ptj/80.9.896

Singh, S.S., Williams, J.J., Hruby, P., Xiao, X., De Carlo, F., Chawla, N., 2014. In situ experimental techniques to study the mechanical behavior of materials using X-ray synchrotron tomography. Integr. Mater. Manuf. Innov. 3, 1–14. https://doi.org/10.1186/2193-9772-3-9

Širka, A., Raina, D.B., Isaksson, H., Tanner, K.E., Smailys, A., Kumar, A., Tarasevičius, Š., Tägil, M., Lidgren, L., 2018. Calcium Sulphate/Hydroxyapatite Carrier for Bone Formation in the Femoral Neck of Osteoporotic Rats. Tissue Eng. Part A 24, 1753–1764. https://doi.org/10.1089/ten.tea.2018.0075

Sobolev, B., Sheehan, K.J., Kuramoto, L., Guy, P., 2015. Risk of second hip fracture persists for years after initial trauma. Bone 75, 72–76. https://doi.org/10.1016/j.bone.2015.02.003

Stravinskas, M., Tarasevicius, S., Laukaitis, S., Nilsson, M., Raina, D.B., Lidgren, L., 2018. A ceramic bone substitute containing gentamicin gives good outcome in trochanteric hip fractures treated with dynamic hip screw and in revision of total hip arthroplasty : a case series. BMC Musculoskelet. Disord. 8, 1–7. https://doi.org/10.1186/s12891-018-2360-8

Sun, H., Liu, C., Li, X., Liu, H., Zhang, W., Yang, H., Li, C., Yang, L., 2020. A novel calcium phosphate–based nanocomposite for the augmentation of cement-injectable cannulated pedicle screws fixation: A cadaver and biomechanical study. J. Orthop. Transl. 20, 56–66. https://doi.org/10.1016/j.jot.2019.08.001

Sutter, E.G., Wall, S.J., Mears, S.C., Belkoff, S.M., 2010. The effect of cement placement on augmentation of the osteoporotic proximal femur. Geriatr. Orthop. Surg. Rehabil. 1, 22–6. https://doi.org/10.1177/2151458510378406

Sutton, M.A., Orteu, J.-J., Schreier, H.W., 2009. Image Correlation for Shape, Motion and Deformation Measurements: Basic Concepts, Theory and Applications. Springer. https://doi.org/10.1007/978-0-387-78747-3_1.

Taddei, F., Schileo, E., Helgason, B., Cristofolini, L., Viceconti, M., 2007. The material mapping strategy influences the accuracy of CT-based finite element models of bones: An evaluation against experimental measurements. Med. Eng. Phys. 29, 973–979. https://doi.org/10.1016/j.medengphy.2006.10.014

Tan, L., Yu, X., Wan, P., Yang, K., 2013. Biodegradable Materials for Bone Repairs: A Review. J. Mater. Sci. Technol. 29, 503–513. https://doi.org/10.1016/j.jmst.2013.03.002

Tang, T., Cripton, P.A., Guy, P., McKay, H.A., Wang, R., 2018. Clinical hip fracture is accompanied by compression induced failure in the superior cortex of the femoral neck. Bone 108, 121–131. https://doi.org/10.1016/j.bone.2017.12.020

Tozzi, G., Dall'Ara, E., Palanca, M., Curto, M., Innocente, F., Cristofolini, L., 2017. Strain uncertainties from two digital volume correlation approaches in prophylactically augmented vertebrae: Local analysis on bone and cement-bone microstructures. J. Mech. Behav. Biomed. Mater. 67, 117–126. https://doi.org/10.1016/j.jmbbm.2016.12.006

Treece, G.M., Gee, A.H., Mayhew, P.M., Poole, K.E.S., 2010. High resolution cortical bone thickness measurement from clinical CT data. Med. Image Anal. 14, 276–290. https://doi.org/10.1016/j.media.2010.01.003

Tudisco, E., Andò, E., Cailletaud, R., Hall, S.A., 2017. TomoWarp2: A local digital volume correlation code. SoftwareX 6, 267–270. https://doi.org/10.1016/j.softx.2017.10.002

Turesson, E., Ivarsson, K., Thorngren, K.G., Hommel, A., 2018. Hip fractures – Treatment and functional outcome. The development over 25 years. Injury 49, 2209–2215. https://doi.org/10.1016/j.injury.2018.10.010

Turner, C.H., Burr, D.B., 1993. Basic biomechanical measurements of bone: A tutorial. Bone 14, 595–608. https://doi.org/10.1016/8756-3282(93)90081-K

Turunen, M.J., Le Cann, S., Tudisco, E., Lovric, G., Patera, A., Hall, S.A., Isaksson, H., 2020. Sub-trabecular strain evolution in human trabecular bone. Sci. Rep. 10. https://doi.org/10.1038/s41598-020-69850-x

Väänänen, S.P., Grassi, L., Flivik, G., Jurvelin, J.S., Isaksson, H., 2015. Generation of 3D shape, density, cortical thickness and finite element mesh of proximal femur from a DXA image. Med. Image Anal. 24, 125–134. https://doi.org/10.1016/j.media.2015.06.001

Väänänen, S.P., Grassi, L., Venäläinen, M.S., Matikka, H., Zheng, Y., Jurvelin, J.S., Isaksson, H., 2019. Automated segmentation of cortical and trabecular bone to generate finite element models for femoral bone mechanics. Med. Eng. Phys. 70, 19–28. https://doi.org/10.1016/j.medengphy.2019.06.015

Van Den Kroonenberg, A.J., Hayes, W.C., McMahon, T.A., 1996. Hip impact velocities and body configurations for voluntary falls from standing height. J. Biomech. 29, 807–811. https://doi.org/10.1016/0021-9290(95)00134-4

Varga, P., Hofmann-Fliri, L., Blauth, M., Windolf, M., 2016. Prophylactic augmentation of the osteoporotic proximal femur—mission impossible? Bonekey Rep. 5, 7270. https://doi.org/10.1038/bonekey.2016.86

Varga, P., Inzana, J.A., Schwiedrzik, J., Zysset, P.K., Gueorguiev, B., Blauth, M., Windolf, M., 2017. New approaches for cement-based prophylactic augmentation of the osteoporotic proximal femur provide enhanced reinforcement as predicted by non-linear finite element simulations. Clin. Biomech. 44, 7–13. https://doi.org/10.1016/j.clinbiomech.2017.03.001

Verhulp, E., van Rietbergen, B., Huiskes, R., 2006. Comparison of micro-level and continuum-level voxel models of the proximal femur. J. Biomech. 39, 2951–2957. https://doi.org/10.1016/j.jbiomech.2005.10.027

Viceconti, M., Hunter, P., Hose, R., 2015. Big Data, Big Knowledge: Big Data for Personalized Healthcare. IEEE J. Biomed. Heal. Informatics 19, 1209–1215. https://doi.org/10.1109/JBHI.2015.2406883

Viceconti, M., Qasim, M., Bhattacharya, P., Li, X., 2018. Correction to: Are CT-Based Finite Element Model Predictions of Femoral Bone Strength Clinically Useful? Curr. Osteoporos. Rep. 1. https://doi.org/10.1007/s11914-018-0466-4

Von Rüden, C., Augat, P., 2016. Failure of fracture fixation in osteoporotic bone. Injury 47, S3–S10. https://doi.org/10.1016/S0020-1383(16)47002-6

Wang, J.S., Tägil, M., Isaksson, H., Boström, M., Lidgren, L., 2016. Tissue reaction and material biodegradation of a calcium sulfate/apatite biphasic bone substitute in rat muscle. J. Orthop. Transl. 6, 10–17. https://doi.org/10.1016/j.jot.2015.11.002

WHO Study Group, 1994. Assessment of fracture risk and its application to screening for postmenopausal osteoporosis. Geneva.

Wolff, J., Heller, M.O., Taylor, W.R., Aslanidis, N., Duda, G.N., 1870. Ueber die innere Architectur der Knochen und ihre Bedeutung für die Frage vom Knochenwachsthum. Virchows Arch Pathol Anat Physiol 50, 389–450. https://doi.org/10.1007/s11999-010

Yang, L., Parimi, N., Orwoll, E.S., Black, D.M., Schousboe, J.T., Eastell, R., 2018. Association of incident hip fracture with the estimated femoral strength by finite element analysis of DXA scans in the Osteoporotic Fractures in Men (MrOS) study. Osteoporos. Int. 29, 643–651. https://doi.org/10.1007/s00198-017-4319-2

Zani, L., Cristofolini, L., Juszczyk, M.M., Grassi, L., Viceconti, M., 2013. A new paradigm for the in vitro simulation of sideways fall loading of the proximal human femur. J. Mech. Med. Biol. 14, 1450005. https://doi.org/10.1142/S0219519414500055

Zani, L., Erani, P., Grassi, L., Taddei, F., Cristofolini, L., 2015. Strain distribution in the proximal Human femur during in vitro simulated sideways fall. J. Biomech. 48, 2130–2143. https://doi.org/10.1016/j.jbiomech.2015.02.022

Zhu, X., Chen, X., Chen, C., Wang, G., Gu, Y., Geng, D., Mao, H., Zhang, Z., Yang, H., 2012. Evaluation of calcium phosphate and calcium sulfate as injectable bone cements in sheep vertebrae. J. Spinal Disord. Tech. 25, 333–337. https://doi.org/10.1097/BSD.0b013e3182213f57

Zysset, P.K., Dall'Ara, E., Varga, P., Pahr, D.H., 2013. Finite element analysis for prediction of bone strength. Bonekey Rep. 2, 1–9. https://doi.org/10.1038/bonekey.2013.120